Impacts of atmospheric transport and biomass burning on the interannual variation in black carbon aerosols over the Tibetan Plateau

Han Han[1,#], Yue Wu[1,2,#], Jane Liu[3,1], Tianliang Zhao[4], Bingliang Zhuang[1], Yichen Li[1], Huimin Chen[1], Ye Zhu[5], Hongnian Liu[1], Qin'geng Wang[6], Shu Li[1], Tijian Wang[1], Min Xie[1], and Mengmeng Li[1]

[1]School of Atmospheric Sciences, Nanjing University, Nanjing, China

[2]Suzhou Meteorological Bureau, Suzhou, China

[3]Department of Geography and Planning, University of Toronto, Toronto, Canada

[4]School of Atmospheric Physics, Nanjing University of Information Science & Technology, Nanjing, China

[5]Shanghai Public Meteorological Service Centre, Shanghai, China

[6]School of the Environment, Nanjing University, Nanjing, China

[#]These authors contributed equally to this work.

Correspondence: Jane Liu (janejj.liu@utoronto.ca)

Abstract

Atmospheric black carbon (BC) in the Tibetan Plateau (TP) can largely impact regional and global climate. Still, studies on the interannual variation in atmospheric BC over the TP and associated variation in BC sources and controlling factors are rather limited. In this study, we characterize the variations in atmospheric BC over the TP surface layer through analysis of 20-year (1995-2014) simulations from a global chemical transport model, GEOS-Chem. The results show that, of all areas in

the TP, surface BC concentrations are highest over the eastern and southern TP, where surface BC are

25   susceptible respectively to BC transport from East Asia and South Asia. Combining the GEOS-Chem

simulations and trajectories from the Hybrid Single-Particle Lagrangian Integrated Trajectory

(HYSPLIT) model, we assess the contributions of different source regions to surface BC in the TP. On

the 20-year average, over 90% surface BC in the TP comes from South Asia (47%) and East Asia (46%).

Regarding seasonal variation in foreign influences, South Asia and East Asia are dominant source

30   regions in winter and summer, respectively, in terms of both magnitude and affected areas in the TP. In

spring and autumn, the influences from the two source regions are somewhat comparable. Interannually,

surface BC over the TP is largely modulated by atmospheric transport of BC from foreign regions year-

round and by biomass burning in South Asia, mostly in spring. We find that the extremely strong

biomass burning in South Asia in the spring of 1999 greatly enhanced surface BC concentrations in the

35   TP (31% relative to the climatology). We find that the strength of the Asian monsoon correlates

significantly with the interannual variation in the amount of BC transported to the TP from foreign

regions. In summer, strong East Asian summer monsoon and South Asian summer monsoon tend to,

respectively, increase BC transport from central China and northeast South Asia to the TP. In winter, BC

transport from central China is enhanced in years with strong East Asia winter monsoon or Siberian

40   High. A strong Siberian High can also increase BC transport from northern South Asia to the TP. This

study underscores the impacts of atmospheric transport and biomass burning on the interannual

variation in surface BC over the TP. It reveals a close connection between the atmospheric transport of

BC from foreign regions to the TP and the Asian monsoon.

1 Introduction

Black carbon (BC) is a carbonaceous aerosol formed from combustion of carbon-based fuels and

materials. BC in the atmosphere is a major air pollutant and a strong absorber of solar radiation (Bond et

al., 2013). Atmospheric BC can greatly influence regional (Ramanathan and Carmichael, 2008; Zhuang et al., 2018) and global (Allen et al., 2012; Chung et al., 2012) climate through multiple mechanisms. It

50   can cause atmospheric heating (Cappa et al., 2012) and surface dimming (Flanner et al., 2009) and influence cloud formation and development processes (Jacobson et al., 2012). Furthermore, after its deposition on snow or ice, BC reduces the surface albedo and accelerates the melting of glaciers and snow cover (Hansen and Nazarenko, 2004; Flanner et al., 2007).

55   The Tibetan Plateau (TP) has an average altitude of over 4 km and an area of 2.6 million km^2, known as the Third Pole. Because of its special geography, the TP can greatly impact regional and global climate through dynamic and thermal processes (Wu et al., 2015; Li et al., 2018). The TP has a large number of glaciers and a wide coverage of snow. Although atmospheric BC in the TP is among the lowest in the world, BC there can alter the climate (Lau et al., 2010; Jiang et al., 2017), ecosystem

60   (Kang et al., 2019), and hydrology (Barnett et al., 2005) in the TP, consequently influencing the living environment of billions of people in the world. Atmospheric BC is an important factor driving the surface warming in the TP due to its strong absorption of solar radiation (He et al., 2014a). After its deposition to the TP ground, BC in the snow reduces the surface albedo (Ming et al., 2009; Qian et al., 2011; Qu et al., 2014) and the duration of snow cover (Ménégoz et al., 2014; Zhang et al., 2018) in the

65   TP. Furthermore, BC in both atmosphere and cryosphere over the TP is responsible for retreats of the snow cover (Menon et al., 2010; Xu et al., 2016) and glaciers (Xu et al., 2009; Ming et al., 2012; Niu et al., 2020).

Atmospheric BC concentrations in the TP vary with location and season, which was revealed by

70   limited observations over different regions in southern (Marinoni et al., 2010; Putero et al., 2014; Chen et al., 2018), northern (Zhao et al., 2012), and southeastern (Cao et al., 2011; Wang et al., 2018, 2019)

TP. Over these regions, seasonal variations in atmospheric BC show different patterns. In the Himalayas over the southern TP, surface BC concentrations were observed to reach the highest in spring and the lowest in summer (Marinoni et al., 2010; Chen et al., 2018). In the Qilian Shan over the northern TP,

75 surface BC concentrations were reported to be highest in summer and lowest in autumn (Zhao et al., 2012). Wang et al. (2016) suggested that surface BC concentrations show a seasonality of winter high and spring low at a site in the southeastern TP, while a pattern of winter low and spring high at a site in the central TP. Few studies have explored the interannual variation in atmospheric BC concentrations over the TP (Mao and Liao, 2016). Since BC observations in the TP are limited due to the harsh

80 environment and sparse sites, numerical modeling on the variation in atmospheric BC over the TP is desirable.

Due to weak anthropogenic activities and biomass burning, the contribution of local emissions to atmospheric BC in the TP is low (Zhang et al., 2015). Concentrations of atmospheric BC in the TP are

85 greatly influenced by the long-range transport of BC from foreign regions (Kopacz et al., 2011; Kang et al., 2019). Previous studies have investigated the pathways of BC transport to the TP (Cao et al., 2011) and some of them suggested that South Asia and East Asia are two main source regions of atmospheric BC in the TP (Lu et al., 2012). The Asian summer monsoon system was identified as an important influencing factor for BC transport from South Asia to the TP (Chen et al., 2013; Han et al., 2014; Xu et

90 al., 2014; Zhang et al., 2015). In summer, BC from northern India can be transported to the middle and upper troposphere and then crossing the Himalayas to the TP via southwesterly winds (Yang et al., 2018). BC emissions in East Asia can also be uplifted to upper layers by summer monsoon circulation and then transported to the northeastern TP (Zhang et al., 2015). The midlatitude westerlies are favorable for BC transport from central Asia and northern India to the western TP (Chen et al., 2018)

95 but unfavorable for BC transport from eastern China to the TP (Cao et al., 2011). Although previous

studies explored the mechanisms of BC transport to the TP, large uncertainties remain in the quantified

fractional contributions of BC transport from different source regions to the TP (Yang et al., 2018).

More importantly, how BC transport to the TP varies interannually and what are underlying mechanisms

for the variation are unclear. Therefore, it is necessary to examine how seasonal BC transport to the TP

100   varies from year to year and whether there is a connection between the Asian monsoon and the

interannual variation in BC transport to the TP.

Observations and simulations showed previously that anthropogenic and fire emissions are major

sources of atmospheric BC in the TP (Lu et al., 2012; Zhang et al., 2015). Zhang et al. (2015) estimated

105   that biomass burning together with biofuel emissions can contribute to around half of the annual mean

BC column burden over the TP. Engling et al. (2011) reported that BC emissions from fire events in

Southeast Asia in spring could probably increase the BC concentrations over a mountain site in the

southeastern part of the TP. Putero et al. (2014) suggested that over half of the high BC episodes in the

southern Himalayas were likely affected by the fire events in South Asia. However, these studies

110   demonstrated the influences of biomass burning in a relative short term or during some fire events, few

investigated the influences in a long term over a decade. The influence of biomass burning on the

interannual variation in atmospheric BC over the TP warrants an in-depth study.

In this study, we aim to assess the impacts of atmospheric transport and biomass burning on

115   surface BC concentrations over the TP, especially on the interannual variation in BC during 1995-2014.

To estimate BC transport from different source regions to the TP, we adopt a numerical approach based

on a global chemical transport model, GEOS-Chem (Bey et al., 2001), and a trajectory model, the

Hybrid Single-Particle Lagrangian Integrated Trajectory model (HYSPLIT) (Draxler and Hess, 1998;

Stein et al., 2015). In the following, the method and models are described in section 2. Section 3

120 discusses the seasonal variations in surface BC over the TP and in BC transport from source regions to

the TP based on the mean status of the 20-year simulations. The interannual variation in surface BC

over the TP and the impacts of biomass burning and transport on this variation are analyzed in section 4.

Conclusions, along with discussion, are provided in section 5. In this paper, BC refers to BC aerosols in

the atmosphere. Surface BC refers to atmospheric BC aerosols in the surface layer.

125

2 Data and methods

2.1 GEOS-Chem simulations

A global chemical transport model, GEOS-Chem (version v9-02, http://geos-chem.org) (Bey et al.,

2001), is used in this study to simulate global BC concentrations. GEOS-Chem is driven by the NASA

130 Modern-Era Retrospective Analysis for Research and Applications (MERRA) meteorological data

(Rienecker et al., 2011). In this study, we focused on how surface BC in the TP responds to interannual

variations in natural processes including biomass burning and meteorology. Therefore, anthropogenic

emissions in our simulation were allowed to vary seasonally but not interannually, i.e. anthropogenic

emissions in 2000 including their seasonality were used for 20 simulation years. We conducted three

135 GEOS-Chem simulations in this study: CTRL, FixBB, and FixMet. The three simulations covered the

period from 1995 to 2014 (using 1994 for spin-up) at 2° latitude by 2.5° longitude horizontal resolution

with 47 vertical layers. In CTRL, both biomass burning emissions and meteorological fields varied

interannually. In FixBB, interannual meteorology was allowed and fire emissions were fixed in 2005, so

to remove the impact of the interannual variation in biomass burning. In FixMet, emissions from

140 biomass burning were allowed to vary interannually and meteorology was fixed in 2005, so to remove

the impact of interannual meteorology.

In the simulations, global anthropogenic BC emissions were based on Bond et al. (2007), with an

annual emission of 4.4 Tg C in 2000 (Leibensperger et al., 2012). Global biomass burning emissions of

145   BC were from the Global Fire Emissions Database version 3 (GFED3) inventory (van der Werf et al.,

2010), which covers the period of 1997-2011. BC in GEOS-Chem is represented by two tracers:

hydrophobic and hydrophilic (Park et al., 2003). Freshly emitted BC is mostly (80%) hydrophobic

(Cooke et al., 1999). Hydrophobic BC becomes hydrophilic typically in a few days (McMeeking et al.,

2011), which is simply assumed as 1.15 days in the model, called an e-folding time (Cooke et al., 1999;

150   Park et al., 2005; He et al., 2014b). Simulations of aerosol dry and wet depositions follows Liu et al.

(2001). Dry deposition of aerosols is simulated using a resistance-in-series model (Walcek et al., 1986)

dependent on local surface type and meteorological conditions, while wet deposition scheme includes

scavenging in convective updrafts, as well as in-cloud and below-cloud scavenging from convective and

large-scale precipitation. Dry deposition is generally smaller than wet deposition (He et al., 2014b; Li et

155   al., 2015). Tracer advection is computed every 15 minutes with a flux-form semi-Lagrangian method

(Lin and Rood, 1996). The tracer moist convection scheme follows Allen et al. (1996a, b), using GEOS

convection, entrainment, and detrainment mass fluxes. The deep convection is parameterized using the

relaxed Arakawa-Schubert scheme (Arakawa and Schubert, 1974; Moorthi and Suarez, 1992) and for

the shallow convection, the scheme in Hack (1994) is used.

160

2.2 GEOS-Chem evaluation

GEOS-Chem simulations of surface BC concentrations were previously evaluated over the TP and

China (He et al., 2014b; Li et al., 2015). Here, we validated the model in the TP and its surrounding

regions for enhanced confidence. As surface BC measurements in the TP are rather limited, the

165   observation data collected at 13 sites (Figure 1) from previous literature (Carrico et al., 2003; Qu et al.,

2008; Zhang et al., 2008; Beegum et al., 2009; Ganguly et al., 2009; Bonasoni et al., 2010; Ming et al.,

2010; Pathak et al., 2010; Ram et al., 2010a, b; Nair et al., 2012) were used in this study, following He

et al. (2014b). The 13 sites were grouped into urban, rural, and remote sites (He et al., 2014b). The

observational data are available for 2006 at 9 of the 13 sites and available at the other sites for different

170   periods, i.e., 1999-2000, 2004-2005 and 2008-2009. BC observations at a remote site during 2015-2017

from another study (Chen et al., 2018) were also used.

The annual mean surface BC concentrations from GEOS-Chem and observations are compared in

Table 1. The observed surface BC concentrations are below 2 μg m^{-3} at remote sites, about 2-5 μg m^{-3} at

175   rural sites, and as high as 5 μg m^{-3} at urban sites (He et al., 2014b). Compared with the observations,

GEOS-Chem performs well at the remote sites, moderately at the rural sites, and poorly at the urban

sites (Table 1). The simulations substantially underestimate surface BC concentrations at the urban sites,

likely due to the coarse horizontal resolution in the model that dilutes the intensity of local emissions in

a model grid. Taking the rural and remote sites only (Figure 2a), we found a high consistency between

180   the annual mean simulations and observations, with a significant correlation coefficient of 0.99. The

comparison suggests that GEOS-Chem can generally capture the spatial variation in surface BC

concentrations over the TP. Moreover, the seasonality of simulated surface BC concentrations was

evaluated at three sites (Figures 2b-2d). GEOS-Chem simulates low BC concentrations in summer and

high BC concentrations in winter and spring at the sites. The amplitude of the seasonal variation in the

185   simulations is weaker than that in the observations. Moorthy et al. (2013) found that simulated surface

BC concentrations by the Goddard Global Ozone Chemistry Aerosol Radiation and Transport

(GOCART) model in winter were lower than the observed ones at a TP site and they attributed this to

the biases in the atmospheric boundary layer parameterization scheme. Wintertime surface BC

concentrations were also underestimated by the Community Atmosphere Model version 5 (CAM5,

190   Zhang et al., 2015), suggesting a common bias in these models.

2.3 Meteorological and fire data

The meteorological data used in this study are the NCEP/NCAR (National Centers for Environmental

Prediction/National Center for Atmospheric Research) reanalysis, available from the Physical Sciences

195   Division of NOAA Earth System Research Laboratory

(https://www.esrl.noaa.gov/psd/data/gridded/data.ncep.reanalysis.surface.html). The data include

geopotential height and wind. The horizontal resolution is $2°$ latitude $\times 2.5°$ longitude.

The nighttime fire count product retrieved from ATSR (Along Track Scanning Radiometer) using

200   Algorithm 2, available from European Space Agency (http://due.esrin.esa.int/page_wfa.php), were used

to verify the biomass burning emissions in the model. ATSR is onboard the Second European Remote-

Sensing Satellite (ERS-2). The spatial resolution of the data is 1 km, and the sensor achieves a global

coverage every three days. The ATSR satellite data with the period of 1997-2011 were gridded to the

GFED3 grids with a resolution of $0.5°\times 0.5°$ in longitude and latitude.

205

2.4 Transport estimation

Combining GEOS-Chem simulations and HYSPLIT (version 4,

http://www.arl.noaa.gov/HYSPLIT_info.php, Draxler and Hess, 1998; Stein et al., 2015) trajectories,

we estimated the contributions of different source regions in the world to surface BC in the TP during

210   1995-2014. HYSPLIT is an atmospheric transport and dispersion model (Fleming et al., 2012),

developed by the Air Resources Laboratory of the National Oceanic and Atmospheric Administration

(NOAA). Meteorological inputs to HYSPLIT are the NCEP/NCAR reanalysis at a resolution of $2.5°$

latitude $\times 2.5°$ longitude. We evenly divided the TP into 70 GEOS-Chem grids. Considering that the

average lifetime of atmospheric BC is about a week, we simulated 7-day backward trajectories

215   originated from each of the 70 grids. The trajectories were initialized four times a day (00, 06, 12 and 18

UTC) during 1995-2014. The starting altitude for the trajectories is 100 m above ground which is within

the typical planetary boundary layer in the TP (Ram et al., 2010b). We divided the world into six regions

(Figure 1b), including central Asia, East Asia, South Asia, Southeast Asia, the region of other Asia,

Europe, and Africa, and the rest of the world. BC concentrations from CTRL simulation were used in

220   the estimation.

        Lu et al. (2012) proposed a novel approach that combined BC emissions with backward trajectories

to quantify the origins of BC in the TP. Modifying Lu et al. (2012)'s approach, we combined BC

concentrations, instead of BC emissions in Lu et al. (2012), with backward trajectories for the same

225   purpose. We assume that BC aerosols have a lifetime of D days and the back trajectories are simulated

for D days ($D=7$ in this study). To make the estimation stable, the amount of BC transported to a TP

surface grid on a day is assumed to be a mean of the BC transport along the backward trajectories

originated from that grid in the past D days, i.e.,

$$BC_{imported} = \frac{\sum_{d=1}^{D} BC_d}{D} \qquad (1)$$

230   where BC_d is the amount of BC that are transported to that TP surface grid along the backward

trajectory on a previous day d ($d=1, 2, \dots D$).

        Equation (1) provides a way to estimate the amount of BC that is transported to the TP from any

model grid outside the TP during a period of interest. For a grid $g_{i,j,k}$, the total amount ($C_{i,j,k}$) of BC

235   transported from $g_{i,j,k}$ to the TP is estimated by

$$C_{i,j,k} = \frac{\sum_{n=1}^{N} c \times v}{D \times M} \qquad (2)$$

where i, j, k are indices for the model grid in longitude, latitude, and altitude coordinates, respectively. n

is an index for the number of trajectories. N is the total number of trajectories that have passed through

the grid $g_{i,j,k}$ during the period of interest, for example, in a month. c is the daily BC concentrations at

240    $g_{i,j,k}$ when trajectory n passing $g_{i,j,k}$, and v is the volume of $g_{i,j,k}$. M is the number of trajectories in a day

(M=4 in this study). Therefore, the total amount of BC transported to the TP ($T_{i,j}$) from the entire

tropospheric column above a surface grid $g_{i,j,0}$ in a source region during the period of interest is assessed

by

$$T_{i,j} = \sum_{k=1}^{K} C_{i,j,k} \qquad (3)$$

245   where K is the number of model layers in the troposphere.

Finally, the amount of BC transported from a source region to the TP surface can be summed up

and the fractional contributions of different source regions to surface BC in the TP can be quantified.

This method is inspired by Lu et al. (2012) and is robust and stable because it is not sensitive to the

250   number of trajectories taken in a day (M) and the number of days taken for the trajectories (D).

Using this method, the amount of BC transported from a source region to the TP surface is

determined by both BC concentrations over that region and the number of trajectories passing through

that region within the tropospheric column. An example of the estimation of BC transport to the TP

255   surface in April 2005 is shown in Figure 3. In this example, BC concentrations are high in central China

around 110°E (Figure 3a). A large number of trajectories pass through central China and finally arrive at

the TP surface (Figure 3b). Therefore, the amount of BC transported from central China to the TP is

high (Figure 3c). In contrast, although trajectories pass through central Asia are also in large numbers,

the amount of BC transported from central Asia to the TP is small (Figure 3c) because of the low BC

260   concentrations over central Asia and the trajectories appear at high altitudes (Figures 3a and 3b).

Atmospheric
Chemistry
and Physics
Discussions

3 Seasonal variations in surface black carbon over the Tibetan Plateau and in black carbon transport to the Tibetan Plateau

BC transport from each of the source regions to the TP surface varies with season. Figure 4 shows the

265   amount of BC transported from each GEOS-Chem grid to the TP surface in the four seasons. Obviously,

surface BC in the TP mainly originates from South Asia and East Asia, especially from the regions near

the southern and eastern borders of the TP, including central China, northeastern South Asia, and

northern South Asia. These spatial distributions of BC contributions from different source regions in the

four seasons are similar to those in Lu et al. (2002). We also found a good agreement (r=0.72, p<0.05)

270   in the estimation of imported BC between this study and Lu et al. (2012) at several sites in the TP,

although our estimates are higher than those from Lu et al. (2012). The back-trajectory approach

modified in this study shows strong performance in identifying the BC source regions for the TP.

The simulated annual mean surface BC concentrations over the entire TP are shown in Figure 5a.

275   The BC concentrations are high along the eastern and southern borders and low in the center of the TP.

BC concentrations over the TP show strong spatial gradient, which is likely due to the blocking of BC

transport by the mountains with high elevations (Cao et al., 2011; Zhao et al., 2017). Figures 5b-5f show

the dominant source regions for the TP in the annual mean and by season. In the annual mean, 93% of

surface BC in the TP comes from South Asia (47%) and East Asia (46%), which are two dominant

280   source regions for the TP as BC aerosols from South Asia and East Asia can impact 64% and 34% areas

of the TP, respectively (Figure 5b). Because of the leeward location of East Asia under prevailing

westerlies, the influence of East Asia is constrained mainly in northern and eastern TP. In winter, South

Asia is the dominant source region for 83% areas of the TP (Figure 5f), while in summer, East Asia is

the dominant source region for 54% areas of the TP (Figure 5d).

285

Atmospheric
Chemistry
and Physics
Discussions

We further divided the TP into five subregions, namely, eastern TP, southern TP, western TP, northern TP, and central TP (Figure 5a). The 20-year means in the subregions show different BC levels, seasonalities, and dominant BC source regions (Figures 5-7). Over the eastern TP, surface BC concentrations are the highest among the five subregions (Figure 6b). Over 75% of surface BC in the eastern TP is transported from East Asia (Figure 7b).

In the southern TP, surface BC concentrations are the 2nd highest among the five subregions, which are high in spring and low in the other seasons (Figure 6c). Such seasonality is likely resulted from the high fire emissions over South Asia in spring, the favorable atmospheric circulation for BC transport to the southern TP in spring, and the strong wet deposition of BC by the monsoon precipitation in summer (Chen et al., 2018). This seasonality is in consistency with observations in previous studies (Marinoni et al., 2010; Cong et al., 2015). South Asia is the dominant source region for surface BC in the southern TP year-round, with fractional contributions of over 85% (Figure 7c). The dominant contribution of South Asia to the southern TP was also suggested in previous studies (He et al., 2014a; Zhang et al., 2015; Yang et al., 2018). The second key source region for the TP is Southeast Asia.

Over the western TP, BC concentrations are the 3rd lowest among the five subregions, with a seasonality of high BC in winter and spring and low BC in summer and autumn (Figure 6d). The higher values in spring and winter agree with the BC measurements at sites in the western Himalayas (Nair et al., 2013). BC transport from South Asia contributes to 93% of surface BC in winter and 76% in summer (Figure 7d). Such seasonality with winter high and summer low in the fractional contribution of South Asia to surface BC over the western TP were also suggested by Zhang et al. (2015).

In the northern TP, BC concentrations are the 2nd lowest among the five subregions, which are at

310   maximum in winter and minimum in spring (Figure 6e). This seasonality is different from an

observational study, which reported that, over the Qilian Shan in the northern TP, surface BC

concentrations are highest in summer and lowest in autumn (Zhao et al., 2012). The dominant source

region for surface BC over the northern TP is South Asia in winter and East Asia in the other seasons

(Figure 7e). Influenced by the prevailing westerlies, source regions west of the TP (central Asia, the

315   region of other Asia, Europe, and Africa in Figure 1b) contribute to surface BC in the western and

northern TP more than to other TP subregions (Figure 7e). Source regions west of the TP can contribute

to 5-11% and 9-17% surface BC in the western and northern TP, respectively (Figures 7d and 7e).

        Among the five subregions, the central TP is with the lowest BC concentrations (Figure 6f). Source

320   regions other than South Asia and East Asia contribute only 5% or less to surface BC in the central TP

(Figure 7f). Seasonally, BC concentrations over the central TP is higher in spring and winter than in

summer and autumn. This simulated seasonality is different from the observed one at a site in the

central TP reported in Wang et al. (2016), who showed that BC concentrations are higher in spring and

lower in winter from November 2012 to June 2013. In spring and winter, South Asia respectively

325   contributes to 72% and 91% surface BC in this subregion. In contract, East Asia contributes to 58%

surface BC there in summer.

4 Interannual variation in surface black carbon over the Tibetan Plateau

4.1 Influences of biomass burning on surface black carbon over the Tibetan Plateau

330   Figure 8 shows the anomalies of surface BC concentrations averaged over the TP from the three GEOS-

Chem simulations. The simulations from CTRL and FixBB are significantly correlated with each other

in all the seasons (r=0.45, p<0.05 in spring, r>0.8, p<0.05 in the other three seasons), indicating the

important role of meteorology in the interannual variation in surface BC concentrations in the TP.

Atmospheric
Chemistry
and Physics
Discussions

Remarkably, in spring (Figure 8a), the correlation coefficient of BC anomalies between CTRL and

335   FixMet simulations reaches 0.87 (p<0.05), indicating the importance of biomass burning to the

interannual variation in BC in spring. The largest anomaly of BC concentrations from CTRL simulation

is in 1999. The comparison between CTRL and FixMet simulations suggests that this strong anomaly is

largely explained by biomass burning. Even if we exclude the extreme year 1999, the correlation

(r=0.77, p<0.05) between CTRL and FixMet simulations remains significant, indicating the strong

340   influence of biomass burning on the variation in surface BC from year to year.

To further examine influence of biomass burning in spring, we integrally analyzed data from ATSR

satellite fire counts, GFED3 fire emissions, and the GEOS-Chem simulations. Both ATSR and GFED3

data show that fires occur frequently over the Indo-Gangetic Plain, central India, and Southeast Asia

345   (Figures 1 and 9). Fire activities in Asia are well described in the GFED3 inventory that is used in the

GEOS-Chem simulations (Figures 9b and 9c). We found the interannual variation in BC anomalies in

the TP from CTRL simulation is significantly correlated to the fire counts in the Indo-Gangetic Plain

(r=0.76, p<0.05), and central India (r=0.67, p<0.05). The correlation was insignificant for Southeast

Asia (r=0.19, p>0.05). In spring of 1999, extreme fire activities occurred in the Indo-Gangetic Plain and

350   central India (Figure 9b). Driven by the favourable atmospheric circulation, the strong BC emissions

from the extremely active fires greatly enhanced surface BC concentrations in the TP (Figure 9d). In the

CTRL simulation, positive BC anomalies appear over the entire TP, with a regional mean of 0.15 μg m^{-3}

or 31% relative to the 1995-2014 climatology (Figure 8a). Additionally, in winter, biomass burning was

extremely strong in 1998 (Figure 8d). The extremely active fires enhanced the regional mean surface

355   BC concentrations in the TP by 0.02 μg m^{-3} or 5% relative to the climatology.

According to Figure 8, the simulations between CTRL and FixMet are not significantly correlated

in summer, autumn, and winter, suggesting that meteorology plays an important role in modulating the

interannual variation in surface BC in the TP. Such a role will be explored in sections 4.2 and 4.3 from

360   the influences of the Asian monsoon on BC transport to the TP in summer and winter, respectively.

4.2 Influences of the Asian summer monsoon on the transport of black carbon to the Tibetan

Plateau

The TP can largely impact the Asian monsoon system through thermal and dynamic processes (Wu et al.,

365   2015). In the meantime, the Asian monsoon can significantly influence the transport of atmospheric

species to the TP (Xu et al., 2014). In this section, we show the influences of two Asian monsoon

subsystems on the interannual variation in BC transport to the TP in summer. We employed a unified

dynamical monsoon index to represent the strength of East Asian summer monsoon (EASM) and South

Asian summer monsoon (SASM). The index was proposed by Li and Zeng (2002) and it has been

370   widely applied to quantify the impact of the Asian monsoon on air pollutants in Asia (Mao et al., 2017;

Lu et al., 2018). Using this index, Han et al. (2019) found a close correlation between the EASM and

ozone transport from foreign regions to East Asia. The calculation of the index was introduced in Li and

Zeng (2002) and Han et al. (2019). The index is respectively termed as EASM index (EASMI) and

SASM index (SASMI), when it is applied to represent the strength of EASM and SASM. A higher

375   EASMI indicates a stronger EASM and a higher SASMI indicates a stronger SASM.

Figure 10a shows the spatial distribution of the correlation between BC transport to the TP and

wind at 850 hPa at each of the grids in summer. As known from Figure 4b, central China is a dominant

source region for the TP in summer, accounting for 63% of the imported BC from East Asia to the TP

380   surface. In Figure 10a, BC from central China correlates significantly with the zonal wind at 850 hPa in

central China (Figure 10a), with a regional mean correlation coefficient of -0.55 (p<0.05). Westward

winds (negative in the zonal component of wind vector) over central China favor BC transport from East Asia to the TP. Furthermore, the EASMI also correlates negatively with the zonal wind at 850 hPa over central China (Figure 10b). When the EASM is stronger, the zonal wind in the monsoon circulation

385   weakens over this region (Yang et al., 2014; Han et al., 2019), suggesting that westward winds may occur more or with higher speed. Therefore, BC transport to the TP from central China is enhanced (Figure 10c), as a significantly positive correlation is found between the strength of the EASM and BC transport from central China to the TP surface (r=0.49, p<0.05) and between the strength of the EASM and BC transport from central China to the eastern TP surface (r=0.48, p<0.05). This is further

390   confirmed by the differences in BC transport to the TP surface between summers with strong and weak EASM (Figure 10d).

How the SASM impacts the BC transport from South Asia over the TP surface in summer is also examined (Figure 11). Serving as a heat source in the Asian summer monsoon system, the TP promotes

395   strong convection and modulates the meridional circulation (Xu et al., 2014). Driven by the meridional circulation, BC in South Asia can be transported northward and upward to the TP. BC transport from northeastern South Asia to the TP accounts for 30% of the total BC transport from South Asia (Figure 4b). Interannually, BC transport from northeastern South Asia is significantly correlated with the meridional wind at 500 hPa (r=0.65, p<0.05, Figure 11a), which is also closely correlated to the strength

400   of the SASM (Figure 11b). In strong SASM years, an anomalous cyclone locates over the northern South Asia at 500 hPa and correspondingly the meridional wind over the northeastern South Asia is increased (Figure 11d). This well explains why the interannual variation in BC transport from northeastern South Asia correlates positively with the strength of the SASM (r=0.55, p<0.05 for the TP, r=0.56, p<0.05 for the STP, Figure 11c). Among all source regions, the differences in BC transport from

405   northeastern South Asia to the TP is largest between summers with strong and weak EASM (Figure 11d).

4.3 Influences of the Asian winter monsoon on the transport of black carbon to the Tibetan Plateau

The Asian winter monsoon is a predominant climate feature in Asia and an important modulator of the distribution and transport of air pollutants (Mao et al., 2017; Zhu et al., 2017). However, the impact of the Asian winter monsoon on the interannual variation in BC transport to the TP scantly studied. In this section, we assess such impact with two climate indices. We measure the intensity of East Asian winter monsoon (EAWM) by an index defined by Jhun and Lee (2004). The EAWM index (EAWMI) represents the EAWM intensity by the meridional wind shear associated with the jet stream in the upper troposphere. It can be calculated by the difference in the regional averaged zonal wind speed at 300 hPa between the areas 27.5-37.5°N, 110-170°E and 50-60°N, 80-140°E. Using the EAWMI, it is found that the EAWM is closely correlated with the interannual variation in pollution transport over East Asia (Li et al., 2016; Han et al., 2019). Furthermore, the Siberian High is a key component of the EAWM system (Wu and Wang, 2002) and its strength can be described using an index defined by Wu and Wang (2002). This Siberian High index (SHI) can be calculated from the regional mean sea level pressure over the area of the Siberian High (40-60°N, 80-120°E). The EAWMI and SHI are highly correlated ($r=0.72$, $p<0.05$).

Figure 12 illustrates a connection between the EAWM and BC transport from East Asia to the TP surface. We mainly focused on BC transport from central China, as this area contributes to 54% of the total BC transport from East Asia to the TP (Figure 4d). BC transport from central China to the TP surface layer correlates significantly with the zonal wind at 850 hPa over central China ($r=-0.73$, $p<0.05$, Figure 12a). The zonal wind over this region is also correlated with the strength of the EAWM ($r=-0.5$, $p<0.05$) and the strength of the Siberian High ($r=-0.65$, $p<0.05$) (Figure 12b). A significant correlation

430   (r=0.59, p<0.05) is found between the strength of the EAWM and BC transport from central China to

the TP surface (Figure 12c). When the EAWM is stronger, the more frequent or stronger westward

winds can enhance BC transport from central China to the TP (Figure 12d).

       A connection between BC transport from South Asia to the TP surface and the Siberian High is

435   shown in Figure 13 for winter. BC over the northern South Asia can be transported efficiently to the TP

by the prevailing subtropical westerlies. Northern South Asia contributes to 70% of BC transported

from South Asia to the TP surface (Figure 4d). The contribution of northern South Asia to surface BC in

the TP is significantly related (r=0.72, p<0.05) to the zonal wind at 500 hPa over the TP (Figure 13a).

The westerlies over the TP are also correlated with the strength of Siberian High (Figure 13b). The

440   elevated zonal wind in the middle troposphere over the TP in winters with strong Siberian High can

enhance the BC transport from northern South Asia to the TP (Figure 13d). Significant correlations are

found between the strength of the Siberian High and BC transport from northern South Asia to the TP

surface (r=0.66, p<0.05) and between the strength of the Siberian High and BC transport from northern

South Asia to the southern TP surface (r=0.65, p<0.05) (Figure 13c). In addition, the contribution of

445   northern South Asia to surface BC in the western TP increases significantly with the meridional wind at

500 hPa over the western TP (r=0.64, p<0.05). The differences in BC transport from northern South

Asia to the TP is largest between winters with strong and weak SHI (Figure 13d).

5 Discussion and conclusions

450   Using a global chemical transport model, GEOS-Chem, we characterized the variation in surface BC

over the TP in 20 years from 1995 to 2014. By comparing with observations available in the literature,

GEOS-Chem simulations show good performance in reproducing the spatial distribution, magnitude,

and seasonal variation in surface BC over the TP. Applying an approach that combines the BC

simulations from GEOS-Chem and backward trajectories from HYSPLIT, we identified the source

455   regions for surface BC in the TP and demonstrated the influences of atmospheric transport and biomass

burning on the interannual variation in surface BC over the TP. The major conclusions, along with

discussion, are drawn as follows.

Based on the 20-year mean, surface BC in the TP is mainly influenced by two source regions: East

460   Asia and South Asia. The influence of East Asia is dominant in summer while the influence of South

Asia is dominant in winter. We divided the TP into five subregions: eastern, southern, western, northern,

and central TP. Surface BC concentrations are higher in the southern and eastern TP than in the other

subregions. Surface BC in the southern and eastern TP comes mainly from South Asia and East Asia,

respectively. Over the western TP, surface BC comes mainly from South Asia. Over the northern TP, the

465   dominant BC source region is South Asia in winter and East Asia in the other seasons. Over the central

TP, the dominant BC source region is East Asia in summer and South Asia in the other seasons.

Interannually, from 1995 to 2014, biomass burning can explain over 75% of the variation in

springtime surface BC concentrations over the TP if biomass burning and meteorology are both

470   considered in GEOS-Chem simulations. Indeed, springtime surface BC in the TP is significantly

correlated to the total number of fire counts over the Indo-Gangetic Plain in South Asia (r=0.76, p<0.05),

according to ATSR satellite data. In the spring of 1999, the extremely strong biomass burning in South

Asia largely elevated surface BC concentrations (0.15 μg m^{-3} or 31% relative to the climatology) over

the TP. We noticed that the strong biomass burning in South Asia in the winter of 1998 also enhanced

475   BC concentrations over the TP.

The interannual variation in surface BC over the TP are greatly influenced by meteorology.

Specifically, the Asian monsoon system alters the long-range transport of BC to the TP by modulating the atmospheric circulation. In summer, when the EASM is stronger, the more frequent or stronger

480 westward wind in the lower troposphere can enhance BC transport from central China to the TP. When the SASM is stronger, the increased meridional wind over the northeastern South Asia in the middle troposphere can enhance BC transport from northeastern South Asia to the TP. In winter, when the EAWM is stronger, the reduced zonal wind in the lower troposphere tends to increase BC transport from central China to the TP. A stronger Siberian High can enhance the zonal wind in the middle troposphere

485 over the TP and consequently increases BC transport from northern South Asia to the TP.

The findings in this study provide an enhanced understanding of the long-range transport of BC to the TP. We comprehensively assessed the BC transport from worldwide source regions to the TP. Our results reveal the source regions of surface BC over the entire TP in the four seasons, which was

490 investigated by limited studies (Zhang et al., 2015). The influences of South Asia and East Asia on the TP were noticed by previous studies. Most of them were focused on limited locations (Cao et al., 2011; Engling et al., 2011; Chen et al., 2018) or in one or few seasons (Zhao et al., 2017; Wang et al., 2018). Here, we further quantified the influence of South Asia and East Asia over the entire TP in the four seasons, in terms of both fractional contribution and affected areas in the TP. Moreover, we identified

495 three key areas within South Asia and East Asia and found that the contribution of BC from there to surface BC in the TP is highest among South Asia and East Asia.

Biomass burning is an important source of atmospheric BC in the TP (Zhang et al., 2015). It was observed that BC emissions from biomass burning in South Asia could be transported to the TP by the

500 atmospheric circulation (Cong et al., 2015), and resulted in high BC episodes in the southern TP (Engling et al., 2011; Putero et al., 2014). Only limited numerical studies explored connections between

biomass burning and surface BC in the TP over a long-term period (Mao and Liao, 2016). Here, we demonstrated that biomass burning is an important driver of the interannual variation in surface BC over the TP in spring. In particular, we found that there were extremely strong fire activities over Indo-

505 Gangetic Plain, central India, and Southeast Asia from 1998 winter to 1999 spring that largely enhanced surface BC concentrations over the entire TP. This extreme anomaly in fire activities and associated influence on BC over the TP may have not been fully documented.

We found that the Asian monsoon system can significantly modulate the interannual variation in

510 BC transport from South Asia and East Asia to the TP. Asian monsoon can influence the atmospheric circulation over the TP and its surroundings (Xu et al., 2014; Han et al., 2019). For summer, previous studies mainly focused on the transport pathway build by the SASM, which can meridionally transport BC from South Asia to the TP (Zhao et al., 2017; Kang et al., 2019). In this study, we further revealed that the EASM can modulate the westward transport of BC from central China to the TP. In winter, the

515 Asian monsoon system also significantly influences the BC transport from northern South Asia and central China to the TP. These results can shed some light on the transport mechanisms of other atmospheric species to the TP, such as water vapour.

Numerical simulations, including backward-trajectory (Ming et al., 2009, 2010; Lu et al., 2012),

520 adjoint (Kopacz et al., 2011), and tagging tracer (Zhang et al., 2015) simulations, have been used to identify BC transport from sources to the TP. Modifying an approach proposed by Lu et al. (2012), we developed an efficient and stable method which shows strong performance in revealing the factional contribution of BC transport from different source regions to the TP by season and year. This method can explicitly show the spatial distribution of the contribution of different source regions to surface BC

525 over the TP. It is feasible for users of a chemical transport model to estimate BC transport from different

source regions to a receptor region if adjoint and tagged modes of the model are unavailable to them.

This study is subject to some limitations. Numerical simulations have advantages of covering large areas over the entire TP and long periods, such as 20 years in this study. GEOS-Chem has been used in

530   multiple studies on BC aerosols over the TP (Kopacz et al., 2011; Lu et al., 2012; He et al., 2014b; Mao and Liao. 2016). However, according to this and earlier studies, there are discrepancies between observations and simulations from GEOS-Chem. He et al. (2014b) suggested that BC aerosols over the TP may be underestimated by GEOS-Chem. A smaller seasonal variation in BC concentrations from simulations than from observations is also revealed in this study. All of these imply uncertainty in

535   simulating the absolute BC concentrations over the TP by GEOS-Chem. Additionally, the simulations are with a resolution of 2° latitude by 2° longitude. Such a resolution may not fully capture processes in the sub-grid scale, such as the mountain-valley wind (Cong et al., 2015). Using regional models at higher resolutions in the future can better describe the terrain effect in the TP. This study is focused on natural drivers (biomass burning and meteorology) that are connective to the interannual variation in

540   BC over the TP. The interannual anthropogenic emissions warrant further studies.

Data availability

The GEOE-Chem model is publicly available at http://geos-chem.org. The HYSPLIT model can be acquired from http://www.arl.noaa.gov/HYSPLIT_info.php. The meteorological and fire data were

545   download from https://www.esrl.noaa.gov/psd/data/gridded/data.ncep.reanalysis.surface.html and https://earth.esa.int/web/guest/home, respectively.

Author contributions

JL, YW, and HH designed the research. HH and YW performed the study. HH, YW, YL, HC, and YZ

Atmospheric
Chemistry
and Physics
Discussions

550 analyzed the data. HH, YW, and JL wrote the paper. TZ, BZ, HL, QW, SL, TW, MX, and ML

contributed insight and comments.

Competing interests

The authors declare no conflict of interest.

555

References

Allen, D. J., Kasibhatla, P., Thompson, A. M., Rood, R. B., Doddridge, B. G., Pickering, K. E., Hudson,

R. D., and Lin, S.-J.: Transport-induced interannual variability of carbon monoxide determined

570 using a chemistry and transport model, J. Geophys. Res.-Atmos., 101, 28655-28669,

https://doi.org/10.1029/96JD02984, 1996a.

Allen, D. J., Rood, R. B., Thompson, A. M., and Hudson, R. D.: Three-dimensional radon 222

calculations using assimilated meteorological data and a convective mixing algorithm, J. Geophys.

Res.-Atmos., 101, 6871-6881, https://doi.org/10.1029/95JD03408, 1996b.

575   Allen, R. J., Sherwood, S. C., Norris, J. R., and Zender, C. S.: Recent Northern Hemisphere tropical

expansion primarily driven by black carbon and tropospheric ozone, Nature, 485, 350-354,

https://doi.org/10.1038/nature11097, 2012.

Arakawa, A. and Schubert, W. H.: Interaction of a cumulus cloud ensemble with the large-scale

environment, Part I, J. Atmos. Sci., 31(3), 674-701, https://doi.org/10.1175/1520-

580   0469(1974)031<0674:IOACCE>2.0.CO;2, 1974.

Barnett, T. P., Adam, J. C., and Lettenmaier, D. P.: Potential impacts of a warming climate on water

availability in snow-dominated regions, Nature, 438, 303-309, https://doi.org/10.1038/nature04141,

2005.

Beegum, S. N., Moorthy, K. K., Babu, S. S., Satheesh, S. K., Vinoj, V., Badarinath, K. V. S., Safai, P. D.,

585   Devara, P. C. S., Singh, S., Vinod, Dumka, U. C., and Pant, P.: Spatial distribution of aerosol black

carbon over India during pre-monsoon season, Atmos. Environ., 43, 1071-1078,

https://doi.org/10.1016/j.atmosenv.2008.11.042, 2009.

Bey, I., Jacob, D. J., Yantosca, R. M., Logan, J. A., Field, B. D., Fiore, A. M., Li, Q., Liu, H. Y., Mickley,

L. J., and Schultz, M. G.: Global modeling of tropospheric chemistry with assimilated meteorology:

590   Model description and evaluation, J. Geophys. Res.-Atmos., 106, 23073-23095,

https://doi.org/10.1029/2001JD000807, 2001.

Bonasoni, P., Laj, P., Marinoni, A., Sprenger, M., Angelini, F., Arduini, J., Bonafè, U., Calzolari, F.,

Colombo, T., Decesari, S., Di Biagio, C., di Sarra, A. G., Evangelisti, F., Duchi, R., Facchini, MC.,

Fuzzi, S., Gobbi, G. P., Maione, M., Panday, A., Roccato, F., Sellegri, K., Venzac, H., Verza, GP.,

595   Villani, P., Vuillermoz, E., and Cristofanelli, P.: Atmospheric Brown Clouds in the Himalayas: first

two years of continuous observations at the Nepal Climate Observatory-Pyramid (5079 m), Atmos.

Chem. Phys., 10, 7515-7531, https://doi.org/10.5194/acp-10-7515-2010, 2010.

Bond, T. C., Bhardwaj, E., Dong, R., Jogani, R., Jung, S., Roden, C., Streets, D. G., and Trautmann, N. M.: Historical emissions of black and organic carbon aerosol from energy-related combustion, 1850-2000, Global Biogeochem. Cy., 21, GB2018, https://doi.org/10.1029/2006GB002840, 2007.

Bond, T. C., Doherty, S. J., Fahey, D. W., Forster, P. M., Berntsen, T., DeAngelo, B. J., Flanner, M. G., Ghan, S., Kärcher, B., Koch, D., Kinne, S., Kondo, Y., Quinn, P. K., Sarofim, M. C., Schultz, M. G., Schulz, M., Venkataraman, C., Zhang, H., Zhang, S., Bellouin, N., Guttikunda, S. K., Hopke, P. K., Jacobson, M. Z., Kaiser, J. W., Klimont, Z., Lohmann, U., Schwarz, J. P., Shindell, D., Storelvmo, T., Warren, S. G., and Zender, C. S.: Bounding the role of black carbon in the climate system: A scientific assessment, J. Geophys. Res.-Atmos., 118, 5380-5552, https://doi.org/10.1002/jgrd.50171, 2013.

Cao, J., Tie, X., Xu, B., Zhao, Z., Zhu, C., Li, G., and Liu, S.: Measuring and modeling black carbon (BC) contamination in the SE Tibetan Plateau, J. Atmos. Chem., 67, 45-60, https://doi.org/10.1007/s10874-011-9202-5, 2011.

Cappa, C. D., Onasch, T. B., Massoli, P., Worsnop, D. R., Bates, T. S., Cross, E. S., Davidovits, P., Hakala, J., Hayden, K. L., Jobson, B. T., Kolesar, K. R., Lack, D. A., Lerner, B. M., Li, S.-M., Mellon, D., Nuaaman, I., Olfert, J. S., Petäjä, T., Quinn, P. K., Song, C., Subramanian, R., Williams, E. J., and Zaveri, R. A.: Radiative absorption enhancements due to the mixing state of atmospheric black carbon, Science, 337, 1078-1081, https://doi.org/10.1126/science.1223447, 2012.

Carrico, C. M., Bergin, M. H., Shrestha, A. B., Dibb, J. E., Gomes, L., and Harris, J. M.: The importance of carbon and mineral dust to seasonal aerosol properties in the Nepal Himalaya, Atmos. Environ., 37, 2811-2824, https://doi.org/10.1016/S1352-2310(03)00197-3, 2003.

Chen, S., Huang, J., Zhao, C., Qian, Y., Leung, L. R., and Yang, B.: Modeling the transport and radiative forcing of Taklimakan dust over the Tibetan Plateau: A case study in the summer of 2006, J. Geophys. Res.-Atmos., 118, 797-812, https://doi.org/10.1002/jgrd.50122, 2013.

Atmospheric
Chemistry
and Physics
Discussions

Chen, X., Kang, S., Cong, Z., Yang, J., and Ma, Y.: Concentration, temporal variation, and sources of black carbon in the Mt. Everest region retrieved by real-time observation and simulation, Atmos. Chem. Phys., 18, 12859-12875, https://doi.org/10.5194/acp-18-12859-2018, 2018.

625   Chung, C. E., Ramanathan, V., and Decremer, D.: Observationally constrained estimates of carbonaceous aerosol radiative forcing, P. Natl. Acad. Sci. USA, 109, 11624-11629, https://doi.org/10.1073/pnas.1203707109, 2012.

Cong, Z., Kang, S., Kawamura, K., Liu, B., Wan, X., Wang, Z., Gao, S., and Fu, P.: Carbonaceous aerosols on the south edge of the Tibetan Plateau: concentrations, seasonality and sources, Atmos.

630   Chem. Phys., 15, 1573-1584, https://doi.org/10.5194/acp-15-1573-2015, 2015.

Cooke, W. F., Liousse, C., Cachier, H., Feichter, J.: Construction of a $1\,^{\circ}\times 1\,^{\circ}$ fossil fuel emission data set for carbonaceous aerosol and implementation and radiative impact in the ECHAM4 model, J. Geophys. Res.-Atmos., 104, 22137-22162, https://doi.org/10.1029/1999JD900187, 1999.

Draxler, R. R. and Hess, G.: An overview of the HYSPLIT_4 modelling system for trajectories, Aust.

635   Meteorol. Mag., 47, 295-308, 1998.

Engling, G., Zhang, Y.-N., Chan, C.-Y., Sang, X.-F., Lin, M., Ho, K.-F., Li, Y.-S., Lin, C.-Y., and Lee, J. J.: Characterization and sources of aerosol particles over the southeastern Tibetan Plateau during the Southeast Asia biomass-burning season, Tellus B, 63, 117-128, https://doi.org/10.1111/j.1600-0889.2010.00512.x, 2011.

640   Flanner, M. G., Zender, C. S., Hess, P. G., Mahowald, N. M., Painter, T. H., Ramanathan, V., and Rasch, P. J.: Springtime warming and reduced snow cover from carbonaceous particles, Atmos. Chem. Phys., 9, 2481-2497, https://doi.org/10.5194/acp-9-2481-2009, 2009.

Flanner, M. G., Zender, C. S., Randerson, J. T., and Rasch, P. J.: Present-day climate forcing and response from black carbon in snow, J. Geophys. Res.-Atmos., 112, D11202,

645   https://doi.org/10.1029/2006JD008003, 2007.

Fleming, Z. L., Monks, P. S., and Manning, A. J.: Review: Untangling the influence of air-mass history
in interpreting observed atmospheric composition, Atmos. Res., 104-105, 1-39,
https://doi.org/10.1016/j.atmosres.2011.09.009, 2012.

Ganguly, D., Ginoux, P., Ramaswamy, V., Winker, D. M., Holben, B. N., and Tripathi, S. N.: Retrieving

650   the composition and concentration of aerosols over the Indo-Gangetic basin using CALIOP and
AERONET data, Geophys. Res. Lett., 36, L13806, https://doi.org/10.1029/2009GL038315, 2009.

Hack, J. J.: Parameterization of moist convection in the National Center for Atmos. Res. community
climate model (CCM2), J. Geophys. Res.-Atmos., 99, 5551-5568,
https://doi.org/10.1029/93JD03478, 1994.

655   Han, H., Liu, J., Yuan, H., Wang, T., Zhuang, B., and Zhang, X.: Foreign influences on tropospheric
ozone over East Asia through global atmospheric transport, Atmos. Chem. Phys., 19, 12495-12514,
https://doi.org/10.5194/acp-19-12495-2019, 2019.

Han, Y., Sun, H., Liu, J., Zhao, T., and Gong, S.: Study on simulated seasonal variations of black carbon
aerosol transport and depositions over the Tibetan Plateau, Journal of Arid Meteorology, 32(3),

660   319-325, https://doi.org/10.11755/j.issn.1006-7639(2014)-03-0319, 2014. (in Chinese)

Hansen, J., and Nazarenko, L.: Soot climate forcing via snow and ice albedos, P. Natl. Acad. Sci. USA,
101, 423-428, https://doi.org/10.1073/pnas.2237157100, 2004.

He, C., Li, Q., Liou, K. N., Takano, Y., Gu, Y., Qi, L., Mao, Y., and Leung, L. R.: Black carbon radiative
forcing over the Tibetan Plateau, Geophys. Res. Lett., 41, 7806-7813,

665   https://doi.org/10.1002/2014GL062191, 2014a.

He, C., Li, Q. B., Liou, K. N., Zhang, J., Qi, L., Mao, Y., Gao, M., Lu, Z., Streets, D. G., Zhang, Q.,
Sarin, M. M., and Ram, K.: A global 3-D CTM evaluation of black carbon in the Tibetan Plateau,
Atmos. Chem. Phys., 14, 7091-7112, https://doi.org/10.5194/acp-14-7091-2014, 2014b.

Jacobson, M. Z.: Investigating cloud absorption effects: Global absorption properties of black carbon,

Atmospheric
Chemistry
and Physics
Discussions

670 tar balls, and soil dust in clouds and aerosols, J. Geophys. Res.-Atmos., 117, D06205,

https://doi.org/10.1029/2011JD017218, 2012.

Jhun, J.-G., and Lee, E.-J.: A new East Asian winter monsoon index and associated characteristics of the

winter monsoon, J. Climate, 17, 711-726, https://doi.org/10.1175/1520-

0442(2004)017<0711:ANEAWM>2.0.CO;2, 2004.

675 Jiang, Y., Yang, X.-Q., Liu, X., Yang, D., Sun, X., Wang, M., Ding, A., Wang, T., and Fu, C.:

Anthropogenic aerosol effects on East Asian winter monsoon: The role of black carbon-induced

Tibetan Plateau warming, J. Geophys. Res.-Atmos., 122, 5883-5902,

https://doi.org/10.1002/2016JD026237, 2017.

Kang, S., Zhang, Q., Qian, Y., Ji, Z., Li, C., Cong, Z., Zhang, Y., Guo, J., Du, W., Huang, J., You, Q.,

680 Panday, A. K., Rupakheti, M., Chen, D., Gustafsson, Ö., Thiemens, M. H., and Qin, D.: Linking

atmospheric pollution to cryospheric change in the Third Pole region: current progress and future

prospects, Natl. Sci. Rev., 6, 796-809, https://doi.org/10.1093/nsr/nwz031, 2019.

Kopacz, M., Mauzerall, D. L., Wang, J., Leibensperger, E. M., Henze, D. K., and Singh, K.: Origin and

radiative forcing of black carbon transported to the Himalayas and Tibetan Plateau, Atmos. Chem.

685 Phys., 11, 2837-2852, https://doi.org/10.5194/acp-11-2837-2011, 2011.

Lau, W. K. M., Kim, M.-K., Kim, K.-M., and Lee, W.-S.: Enhanced surface warming and accelerated

snow melt in the Himalayas and Tibetan Plateau induced by absorbing aerosols, Environ. Res. Lett.,

5, 025204, https://doi.org/10.1088/1748-9326/5/2/025204, 2010.

Leibensperger, E. M., Mickley, L. J., Jacob, D. J., Chen, W.-T., Seinfeld, J. H., Nenes, A., Adams, P. J.,

690 Streets, D. G., Kumar, N., and Rind, D.: Climatic effects of 1950-2050 changes in US

anthropogenic aerosols - Part 1: Aerosol trends and radiative forcing, Atmos. Chem. Phys., 12,

3333-3348, https://doi.org/10.5194/acp-12-3333-2012, 2012.

Li, J., and Zeng, Q.: A unified monsoon index, Geophys. Res. Lett., 29, 115-111-115-114,

https://doi.org/10.1029/2001GL013874, 2002.

695   Li, Q., Zhang, R., and Wang, Y.: Interannual variation of the wintertime fog-haze days across central and eastern China and its relation with East Asian winter monsoon, Int. J. Climatol., 36, 346-354, https://doi.org/10.1002/joc.4350, 2016.

Li, W., Guo, W., Qiu, B., Xue, Y., Hsu, P.-C., and Wei, J.: Influence of Tibetan Plateau snow cover on East Asian atmospheric circulation at medium-range time scales, Nat. Commun., 9, 4243,

700   https://doi.org/10.1038/s41467-018-06762-5, 2018.

Li, W. J., Chen, S. R., Xu, Y. S., Guo, X. C., Sun, Y. L., Yang, X. Y., Wang, Z. F., Zhao, X. D., Chen, J. M., and Wang, W. X.: Mixing state and sources of submicron regional background aerosols in the northern Qinghai-Tibet Plateau and the influence of biomass burning, Atmos. Chem. Phys., 15, 13365-13376, https://doi.org/10.5194/acp-15-13365-2015, 2015.

705   Lin, S. J. and Rood, R. B.: Multidimensional flux-form semi-Lagrangian transport schemes, Mon. Wea. Rev., 124(9), 2046-2070, https://doi.org/10.1175/1520-0493(1996)124<2046:MFFSLT>2.0.CO;2, 1996.

Liu, H., Jacob, D. J., Bey, I., and Yantosca, R. M.: Constraints from 210Pb and 7Be on wet deposition and transport in a global three-dimensional chemical tracer model driven by assimilated

710   meteorological fields, J. Geophys. Res.-Atmos., 106, 12109-12128, https://doi.org/10.1029/2000JD900839, 2001.

Lu, X., Zhang, L., Liu, X., Gao, M., Zhao, Y., and Shao, J.: Lower tropospheric ozone over India and its linkage to the South Asian monsoon, Atmos. Chem. Phys., 18, 3101-3118, https://doi.org/10.5194/acp-18-3101-2018, 2018.

715   Lu, Z., Streets, D. G., Zhang, Q., and Wang, S.: A novel back-trajectory analysis of the origin of black carbon transported to the Himalayas and Tibetan Plateau during 1996-2010, Geophys. Res. Lett., 39, L01809, https://doi.org/10.1029/2011GL049903, 2012.

Mao, Y.-H., and Liao, H.: Impacts of meteorological parameters and emissions on decadal, interannual, and seasonal variations of atmospheric black carbon in the Tibetan Plateau, Adv. Climate Change

720   Res., 7, 123-131, https://doi.org/10.1016/j.accre.2016.09.006, 2016.

Mao, Y.-H., Liao, H., and Chen, H.-S.: Impacts of East Asian summer and winter monsoons on interannual variations of mass concentrations and direct radiative forcing of black carbon over eastern China, Atmos. Chem. Phys., 17, 4799-4816, https://doi.org/10.5194/acp-17-4799-2017, 2017.

725 Marinoni, A., Cristofanelli, P., Laj, P., Duchi, R., Calzolari, F., Decesari, S., Sellegri, K., Vuillermoz, E., Verza, G. P., Villani, P., and Bonasoni, P.: Aerosol mass and black carbon concentrations, a two year record at NCO-P (5079 m, Southern Himalayas), Atmos. Chem. Phys., 10, 8551-8562, https://doi.org/10.5194/acp-10-8551-2010, 2010.

McMeeking, G. R., Good, N., Petters, M. D., McFiggans, G., and Coe, H.: Influences on the fraction of

730   hydrophobic and hydrophilic black carbon in the atmosphere, Atmos. Chem. Phys., 11, 5099-5112, https://doi.org/10.5194/acp-11-5099-2011, 2011.

Ménégoz, M., Krinner, G., Balkanski, Y., Boucher, O., Cozic, A., Lim, S., Ginot, P., Laj, P., Gallée, H., Wagnon, P., Marinoni, A., and Jacobi, H. W.: Snow cover sensitivity to black carbon deposition in the Himalayas: from atmospheric and ice core measurements to regional climate simulations,

735   Atmos. Chem. Phys., 14, 4237-4249, https://doi.org/10.5194/acp-14-4237-2014, 2014.

Menon, S., Koch, D., Beig, G., Sahu, S., Fasullo, J., and Orlikowski, D.: Black carbon aerosols and the third polar ice cap, Atmos. Chem. Phys., 10, 4559-4571, https://doi.org/10.5194/acp-10-4559-2010, 2010.

Ming, J., Xiao, C., Cachier, H., Qin, D., Qin, X., Li, Z., and Pu, J.: Black Carbon (BC) in the snow of

740   glaciers in west China and its potential effects on albedos, Atmos. Res., 92, 114-123, https://doi.org/10.1016/j.atmosres.2008.09.007, 2009.

Ming, J., Xiao, C., Sun, J., Kang, S., and Bonasoni, P.: Carbonaceous particles in the atmosphere and
    precipitation of the Nam Co region, central Tibet, J. Environ. Sci., 22, 1748-1756,
    https://doi.org/10.1016/S1001-0742(09)60315-6, 2010.

745   Ming, J., Du, Z., Xiao, C., Xu, X., and Zhang, D.: Darkening of the mid-Himalaya glaciers since 2000
    and the potential causes, Environ. Res. Lett., 7, 014021, https://doi.org/10.1088/1748-
    9326/7/1/014021, 2012.

Moorthi, S. and Suarez, M. J.: Relaxed Arakawa-Schubert. A parameterization of moist convection for
    general circulation models, Mon. Wea. Rev., 120(6), 97-102, https://doi.org/10.1175/1520-
750   0493(1992)120<0978:RASAPO>2.0.CO;2, 1992.

Moorthy, K. K., Beegum, S. N., Srivastava, N., Satheesh, S. K., Chin, M., Blond, N., Babu, S. S., and
    Singh, S.: Performance evaluation of chemistry transport models over India, Atmos. Environ., 71,
    210-225, https://doi.org/10.1016/j.atmosenv.2013.01.056, 2013.

Nair, V. S., Solmon, F., Giorgi, F., Mariotti, L., Babu, S. S., and Moorthy, K. K.: Simulation of South
755   Asian aerosols for regional climate studies, J. Geophys. Res.-Atmos., 117, D04209,
    https://doi.org/10.1029/2011JD016711, 2012.

Nair, V. S., Babu, S. S., Moorthy, K. K., Sharma, A. K., Marinoni, A., and Ajai: Black carbon aerosols
    over the Himalayas: direct and surface albedo forcing, Tellus B, 65, 19738,
    https://doi.org/10.3402/tellusb.v65i0.19738, 2013.

760   Niu, H., Kang, S., Wang, H., Du, J., Pu, T., Zhang, G., Lu, X., Yan, X., Wang, S., and Shi, X.: Light-
    absorbing impurities accelerating glacial melting in southeastern Tibetan Plateau, Environ. Pollut.,
    257, 113541, https://doi.org/10.1016/j.envpol.2019.113541, 2020.

Park, R. J., Jacob, D. J., Chin, M., and Martin, R. V.: Sources of carbonaceous aerosols over the United
    States and implications for natural visibility, J. Geophys. Res.-Atmos., 108(D12), 4355,
765   https://doi.org/10.1029/2002JD003190, 2003.

Atmospheric
Chemistry
and Physics
Discussions

Open Access

EGU

Park, R. J., Jacob, D. J., Palmer, P. I., Clarke, A. D., Weber, R. J., Zondlo, M. A., Eisele, F. L., Bandy, A. R., Thornton, D. C., Sachse, G. W., and Bond, T. C.: Export efficiency of black carbon aerosol in continental outflow: Global implications, J. Geophys. Res.-Atmos., 110, D11205, https://doi.org/10.1029/2004JD005432, 2005.

770   Pathak, B., Kalita, G., Bhuyan, K., Bhuyan, P. K., and Moorthy, K. K.: Aerosol temporal characteristics and its impact on shortwave radiative forcing at a location in the northeast of India, J. Geophys. Res.-Atmos., 115, D19204, https://doi.org/10.1029/2009JD013462, 2010.

Putero, D., Landi, T. C., Cristofanelli, P., Marinoni, A., Laj, P., Duchi, R., Calzolari, F., Verza, G. P., and Bonasoni, P.: Influence of open vegetation fires on black carbon and ozone variability in the

775   southern Himalayas (NCO-P, 5079 m a.s.l.), Environ. Pollut., 184, 597-604, https://doi.org/10.1016/j.envpol.2013.09.035, 2014.

Qian, Y., Flanner, M. G., Leung, L. R., and Wang, W.: Sensitivity studies on the impacts of Tibetan Plateau snowpack pollution on the Asian hydrological cycle and monsoon climate, Atmos. Chem. Phys., 11, 1929-1948, https://doi.org/10.5194/acp-11-1929-2011, 2011.

780   Qu, B., Ming, J., Kang, S.-C., Zhang, G.-S., Li, Y.-W., Li, C.-D., Zhao, S.-Y., Ji, Z.-M., and Cao, J.-J.: The decreasing albedo of the Zhadang glacier on western Nyainqentanglha and the role of light-absorbing impurities, Atmos. Chem. Phys., 14, 11117-11128, https://doi.org/10.5194/acp-14-11117-2014, 2014.

Qu, W. J., Zhang, X. Y., Arimoto, R., Wang, D., Wang, Y. Q., Yan, L. W., and Li, Y.: Chemical

785   composition of the background aerosol at two sites in southwestern and northwestern China: potential influences of regional transport, Tellus B, 60, 657-673, https://doi.org/10.1111/j.1600-0889.2008.00342.x, 2008.

Ram, K., Sarin, M. M., and Hegde, P.: Long-term record of aerosol optical properties and chemical composition from a high-altitude site (Manora Peak) in Central Himalaya, Atmos. Chem. Phys., 10,

790   11791-11803, https://doi.org/10.5194/acp-10-11791-2010, 2010a.

Ram, K., Sarin, M. M., and Tripathi, S. N.: A 1 year record of carbonaceous aerosols from an urban site in the Indo-Gangetic Plain: Characterization, sources, and temporal variability, J. Geophys. Res.-Atmos., 115, D24313, https://doi.org/10.1029/2010JD014188, 2010b.

Ramanathan, V., and Carmichael, G.: Global and regional climate changes due to black carbon, Nat.

795   Geosci., 1, 221-227, https://doi.org/10.1038/ngeo156, 2008.

Stein, A. F., Draxler, R. R., Rolph, G. D., Stunder, B. J. B., Cohen, M. D., and Ngan, F.: NOAA's HYSPLIT atmospheric transport and dispersion modeling system, B. Am. Meteorol. Soc., 96, 2059-2077, https://doi.org/10.1175/BAMS-D-14-00110.1, 2015.

van der Werf, G. R., Randerson, J. T., Giglio, L., Collatz, G. J., Mu, M., Kasibhatla, P. S., Morton, D. C.,

800   DeFries, R. S., Jin, Y., and van Leeuwen, T. T.: Global fire emissions and the contribution of deforestation, savanna, forest, agricultural, and peat fires (1997-2009), Atmos. Chem. Phys., 10, 11707-11735, https://doi.org/10.5194/acp-10-11707-2010, 2010.

Walcek, C. J., Brost, R. A., Chang, J. S., and Wesely, M. L.: SO_2, sulfate and HNO_3 deposition velocities computed using regional landuse and meteorological data, Atmos. Environ. (1967), 20,

805   949-964, https://doi.org/10.1016/0004-6981(86)90279-9, 1986.

Wang, M., Xu, B., Wang, N., Cao, J., Tie, X., Wang, H., Zhu, C., and Yang, W.: Two distinct patterns of seasonal variation of airborne black carbon over Tibetan Plateau, Sci. Total Environ., 573, 1041-1052, https://doi.org/10.1016/j.scitotenv.2016.08.184, 2016.

Wang, M., Xu, B., Yang, S., Gao, J., Zhang, T., He, Z., Kobal, M., and Hansen, A. D. A.: Black carbon

810   profiles from tethered balloon flights over the southeastern Tibetan Plateau (in Chinese), Chin. Sci. Bull., 64, 2949-2958, https://doi.org/10.1360/TB-2019-0101, 2019.

Wang, Q., Cao, J., Han, Y., Tian, J., Zhu, C., Zhang, Y., Zhang, N., Shen, Z., Ni, H., Zhao, S., and Wu, J.: Sources and physicochemical characteristics of black carbon aerosol from the southeastern Tibetan

Plateau: internal mixing enhances light absorption, Atmos. Chem. Phys., 18, 4639-4656,

815   https://doi.org/10.5194/acp-18-4639-2018, 2018.

Wu, B., and Wang, J.: Winter Arctic Oscillation, Siberian High and East Asian winter monsoon,

Geophys. Res. Lett., 29, 3-1-3-4, https://doi.org/10.1029/2002GL015373, 2002.

Wu, G., Duan, A., Liu, Y., Mao, J., Ren, R., Bao, Q., He, B., Liu, B., and Hu, W.: Tibetan Plateau

climate dynamics: recent research progress and outlook, Natl. Sci. Rev., 2, 100-116,

820   https://doi.org/10.1093/nsr/nwu045, 2015.

Xu, B., Cao, J., Hansen, J., Yao, T., Joswia, D. R., Wang, N., Wu, G., Wang, M., Zhao, H., Yang, W., Liu,

X., and He, J.: Black soot and the survival of Tibetan glaciers, P. Natl. Acad. Sci. USA, 106,

22114-22118, https://doi.org/10.1073/pnas.0910444106, 2009.

Xu, X., Zhao, T., Lu, C., Guo, Y., Chen, B., Liu, R., Li, Y., and Shi, X.: An important mechanism

825   sustaining the atmospheric "water tower" over the Tibetan Plateau, Atmos. Chem. Phys., 14,

11287-11295, https://doi.org/10.5194/acp-14-11287-2014, 2014.

Xu, Y., Ramanathan, V., and Washington, W. M.: Observed high-altitude warming and snow cover

retreat over Tibet and the Himalayas enhanced by black carbon aerosols, Atmos. Chem. Phys., 16,

1303-1315, https://doi.org/10.5194/acp-16-1303-2016, 2016.

830 Yang, J., Kang, S., Ji, Z., and Chen, D.: Modeling the origin of anthropogenic black carbon and its

climatic effect over the Tibetan Plateau and surrounding regions, J. Geophys. Res.-Atmos., 123,

671-692, https://doi.org/10.1002/2017JD027282, 2018.

Yang, Y., Liao, H., and Li, J.: Impacts of the East Asian summer monsoon on interannual variations of

summertime surface-layer ozone concentrations over China, Atmos. Chem. Phys., 14, 6867-6879,

835   https://doi.org/10.5194/acp-14-6867-2014, 2014.

Zhang, R., Wang, H., Qian, Y., Rasch, P. J., Easter, R. C., Ma, P.-L., Singh, B., Huang, J., and Fu, Q.:

Quantifying sources, transport, deposition, and radiative forcing of black carbon over the

Himalayas and Tibetan Plateau, Atmos. Chem. Phys., 15, 6205-6223, https://doi.org/10.5194/acp-15-6205-2015, 2015.

840   Zhang, X. Y., Wang, Y. Q., Zhang, X. C., Guo, W., and Gong, S. L.: Carbonaceous aerosol composition over various regions of China during 2006, J. Geophys. Res.-Atmos., 113, D14111, https://doi.org/10.1029/2007JD009525, 2008.

Zhang, Y., Kang, S., Sprenger, M., Cong, Z., Gao, T., Li, C., Tao, S., Li, X., Zhong, X., Xu, M., Meng, W., Neupane, B., Qin, X., and Sillanpää, M.: Black carbon and mineral dust in snow cover on the

845   Tibetan Plateau, The Cryosphere, 12, 413-431, https://doi.org/10.5194/tc-12-413-2018, 2018.

Zhao, S., Ming, J., Xiao, C., Sun, W., and Qin, X.: A preliminary study on measurements of black carbon in the atmosphere of northwest Qilian Shan, J. Environ. Sci., 24, 152-159, https://doi.org/10.1016/S1001-0742(11)60739-0, 2012.

Zhao, S., Tie, X., Long, X., and Cao, J.: Impacts of Himalayas on black carbon over the Tibetan Plateau

850   during summer monsoon, Sci. Total Environ., 598, 307-318, https://doi.org/10.1016/j.scitotenv.2017.04.101, 2017.

Zhu, Y., Liu, J., Wang, T., Zhuang, B., Han, H., Wang, H., Chang, Y., and Ding, K.: The impacts of meteorology on the seasonal and interannual variabilities of ozone transport from North America to East Asia, J. Geophys. Res., 122, 10612–10636, https://doi.org/10.1002/2017JD026761, 2017.

855   Zhuang, B. L., Li, S., Wang, T. J., Liu, J., Chen, H. M., Chen, P. L., Li, M. M., and Xie, M.: Interaction between the Black Carbon Aerosol Warming Effect and East Asian Monsoon Using RegCM4, J. Climate, 31, 9367-9388, https://doi.org/10.1175/JCLI-D-17-0767.1, 2018.

Atmospheric
Chemistry
and Physics
Discussions

Table 1. Comparison between observed and simulated annual mean surface BC concentrations (in μg m^{-3}) during the corresponding periods at various urban, rural, and remote sites (see Figure 1a) over the TP and its surrounding regions.

Site category	Site name	Latitude (ºN)	Longitude (ºE)	Altitude (m)	Time period	Observed BC (μg m^{-3})	Simulated BC (μg m^{-3})	References
Remote	Nagarkot	27.7	85.5	2150	1999-2000	1.0	1.26	Carrico et al. (2003)
	NCOP	28.0	86.8	5079	2006	0.2	0.52	Bonasoni et al. (2010)
	Manora Peak	29.4	79.5	1950	2006	1.13	0.86	Ram et al. (2010a)
	NCOS	30.8	91.0	4730	2006	0.14	0.19	Ming et al. (2010)
	Langtang	28.1	85.6	3920	1999-2000	0.41	0.6	Carrico et al. (2003)
	Zhuzhang	28.0	99.7	3583	2004-2005	0.35	0.26	Qu et al. (2008)
Rural	Kharagpur	22.5	87.5	28	2006	5.56	4.45	Nair et al. (2012)
	Kanpur	26.4	80.3	142	2006	3.77	2.48	Ram et al. (2010b)
	Gandhi College	25.9	84.1	158	2006	4.88	4.05	Ganguly et al. (2009)
Urban	Delhi	28.6	77.2	260	2006	13.59	2.92	Beegum et al. (2009)
	Dibrugarh	27.3	94.6	111	2008-2009	8.91	1.13	Pathak et al. (2010)
	Lhasa	29.7	91.1	3663	2006	3.711	0.19	Zhang et al. (2008)
	Dunhuang	40.2	94.7	1139	2006	4.111	0.18	Zhang et al. (2008)

Atmospheric
Chemistry
and Physics
Discussions
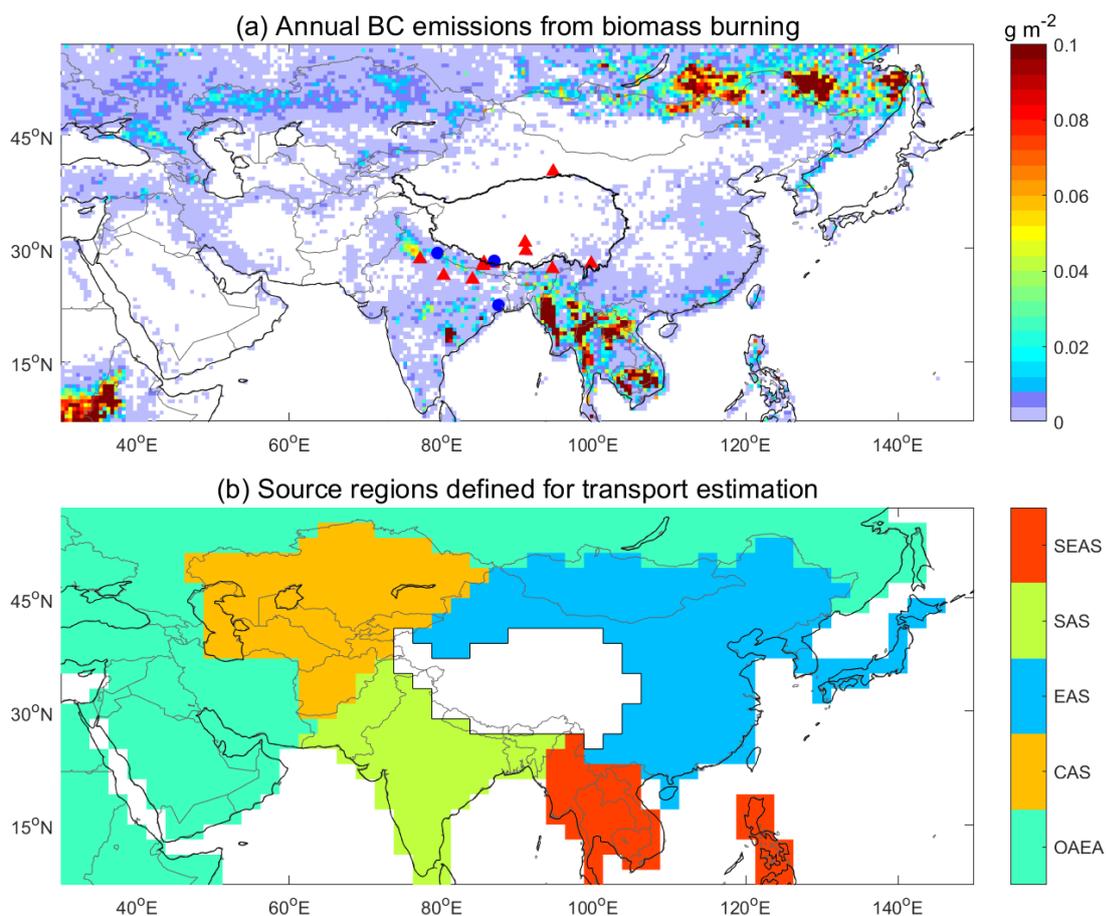
Figure 1. (a) Annual BC emissions from biomass burning averaged over 1997-2011 from GFED3. Red triangles (for Table 1) and blue dots (for Table 1 and Figure 2) indicate the locations of the observation sites used for model evaluation. (b) Source regions defined for the estimation of BC transport to the TP. The abbreviations are for central Asia (CAS), East Asia (EAS), South Asia (SAS), Southeast Asia (SEAS), and the region of other Asia, Europe, and Africa (OAEA). The dark black line in (a) encloses the domain of the TP, corresponding the white areas in (b).
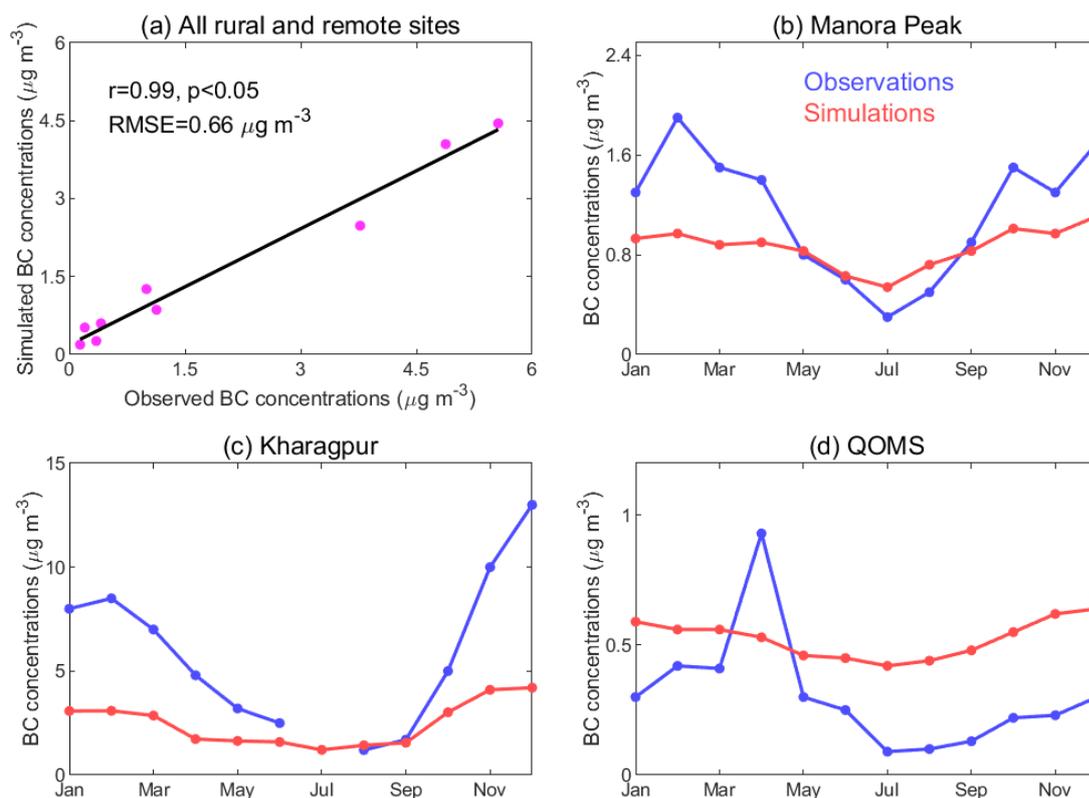
Figure 2. (a) Annual means of the observed and simulated surface BC concentrations at the rural and remote sites (see Table 1) in the TP and its surrounding regions in 2006. Comparisons between the monthly observations and simulations at (b) Manora Peak, (c) Kharagpur, and (d) QOMS (blue dots in Figure 1a) in 2006. Correlation coefficient (*r*) and root mean square error (RMSE) between the observed and simulated BC at all the rural and remote sites are also shown in (a). Observations at QOMS (28.36°N, 86.95°E, 4276 m) are from Chen et al. (2018).
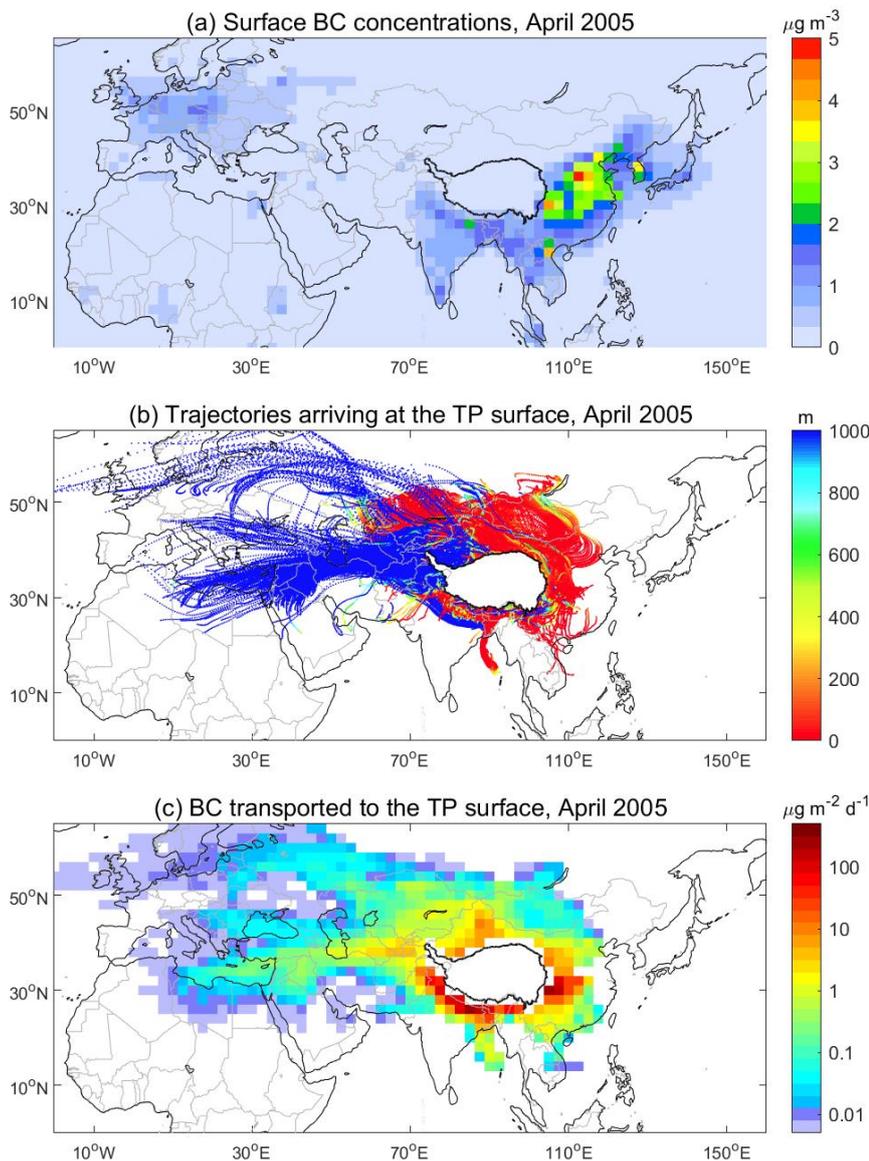
Figure 3. An example of the estimation of BC transport to the TP surface in April 2005. (a) Surface BC concentrations (in $\mu g\ m^{-3}$). (b) 7-day backward trajectories (in meters above the ground) arriving at the TP surface. (c) The amount of BC transported to the TP surface from source regions (in $\mu g\ m^{-2}\ d^{-1}$). The dark black line encloses the domain of the TP.
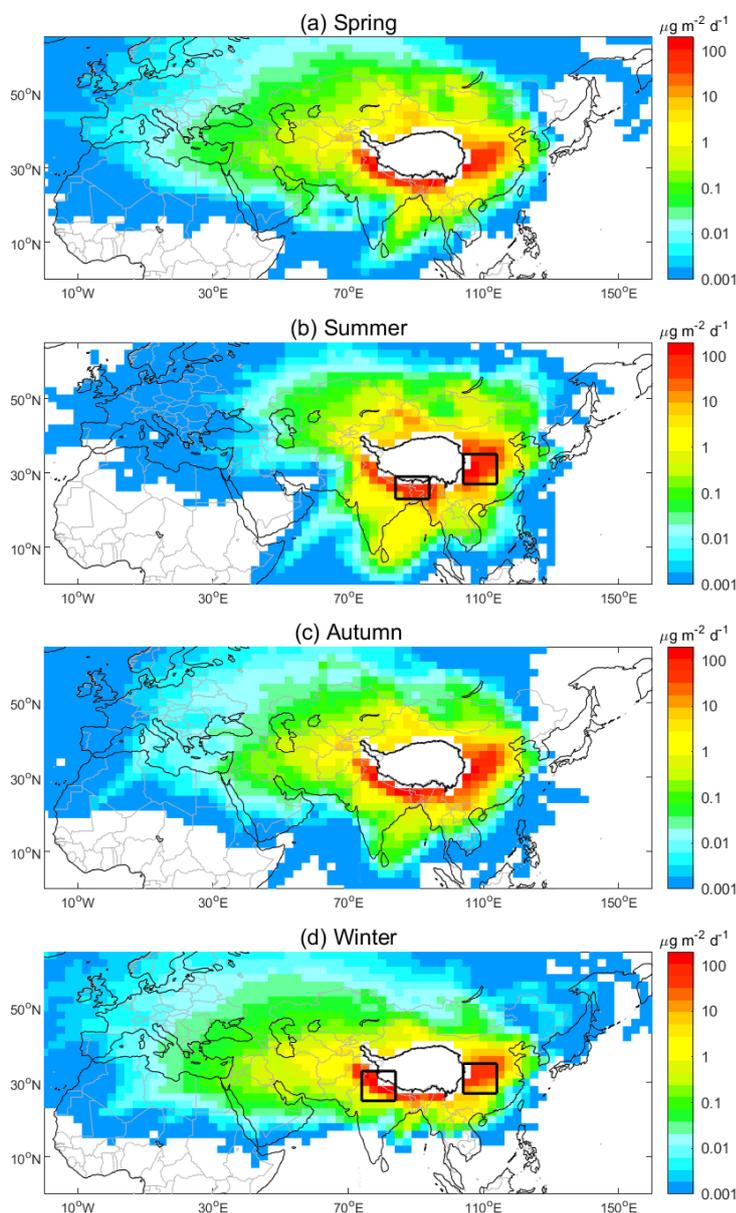
Figure 4. The amount of BC transported to the TP surface (in µg m^{-2} d^{-1}) from source regions in (a) spring, (b) summer, (c) autumn, and (d) winter. The values are based on 20-year (1995-2014) means from CTRL simulation. The boxed areas in (b) indicate central China (CCH; 27-35ºN, 104-114ºE) and northeastern South Asia (NESAS; 23-29ºN, 84-94ºE). The boxed areas in (d) indicate CCH and northern South Asia (NSAS; 25-33ºN, 74-84ºE). The dark black line encloses the domain of the TP.
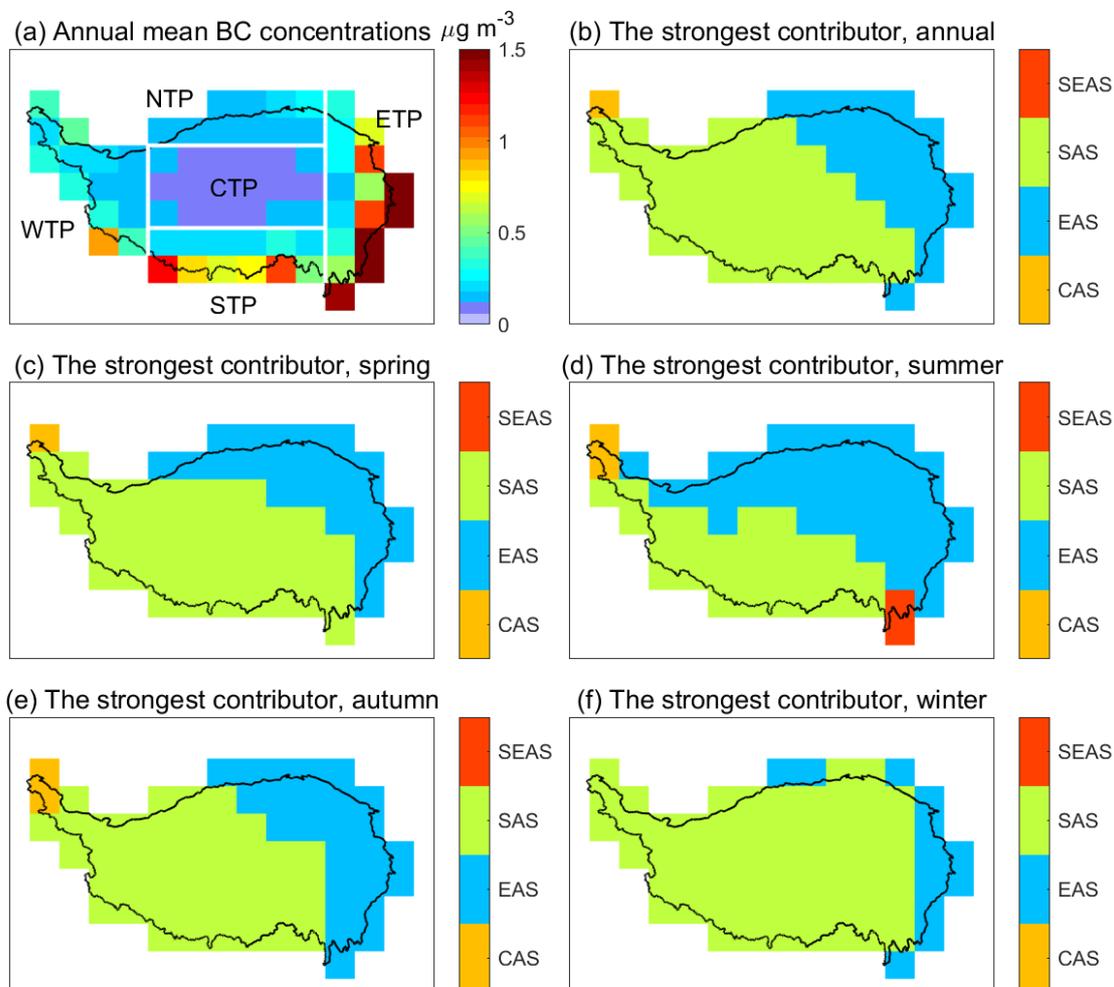
Figure 5. Surface BC over the TP and the dominant BC source regions for the TP. (a) Annual mean BC concentrations over the TP. (b-f) The dominant BC source regions (Figure 1b) for each model grid in the TP for (b) the annual mean, (c) spring, (d) summer, (e) autumn, and (f) winter. The values are 20-year mean (1995-2014) from CTRL simulation. Source regions in (b)-(f) include central Asia (CAS), East Asia (EAS), South Asia (SAS), and Southeast Asia (SEAS). The white solid lines in (a) separate the subregions of the TP defined in this study, i.e., western TP (WTP), northern TP (NTP), central TP (CTP), southern TP (STP), and eastern TP (ETP). The dark black line encloses the domain of the TP.

985

990

995
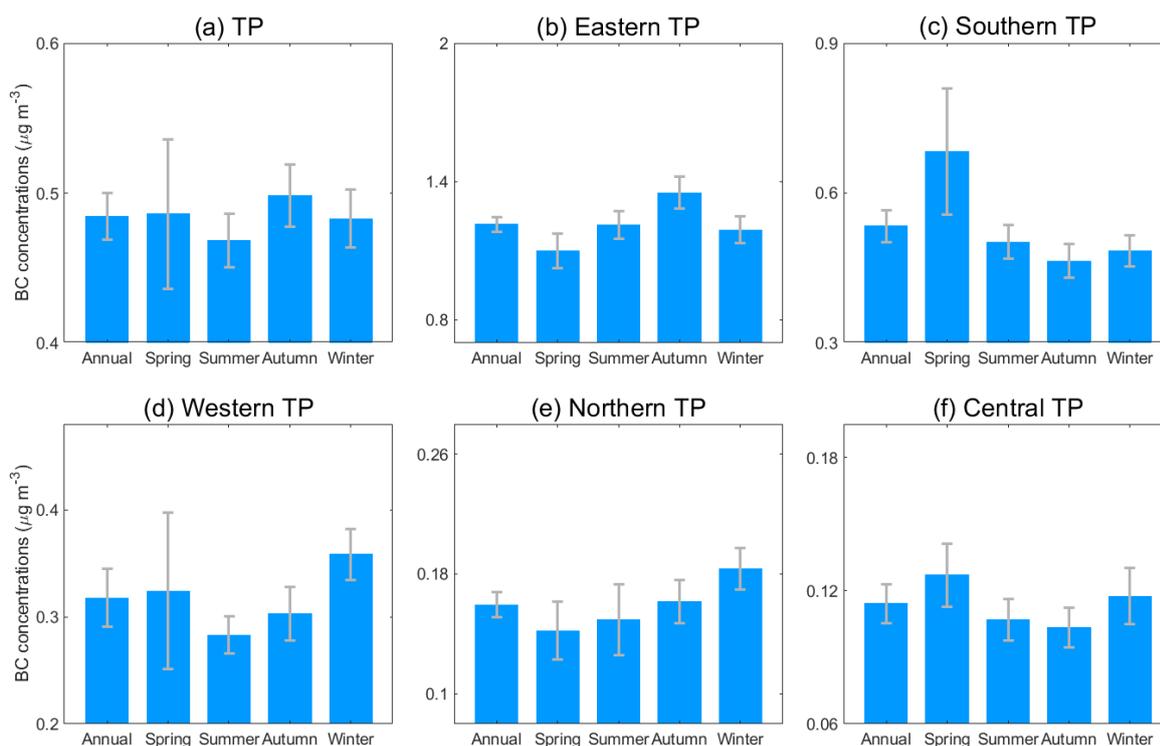
Figure 6. Seasonal variations of surface BC concentrations averaged over the TP and its subregions. The values are 20-year (1995 -2014) means from CTRL simulation. The error bars indicate the standard deviation. Note the y-scales are different for different subregions, ranging from the largest in eastern TP to the smallest in central TP.

1000

Atmospheric
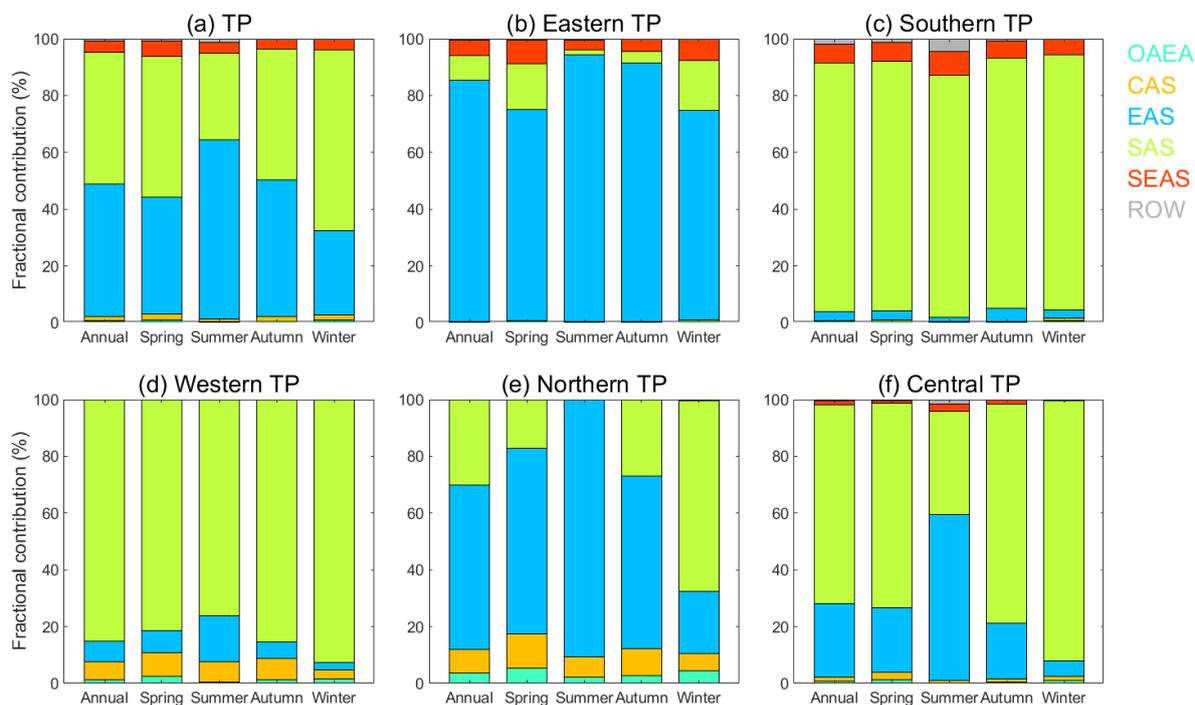Chemistry
and Physics
Discussions

Figure 7. Fractional contributions of different source regions to surface BC over the TP and its subregions. The abbreviations are for central Asia (CAS), East Asia (EAS), South Asia (SAS), Southeast Asia (SEAS), the region of other Asia, Europe, and Africa (OAEA), and rest of the world (ROW).

1025

1030

1035
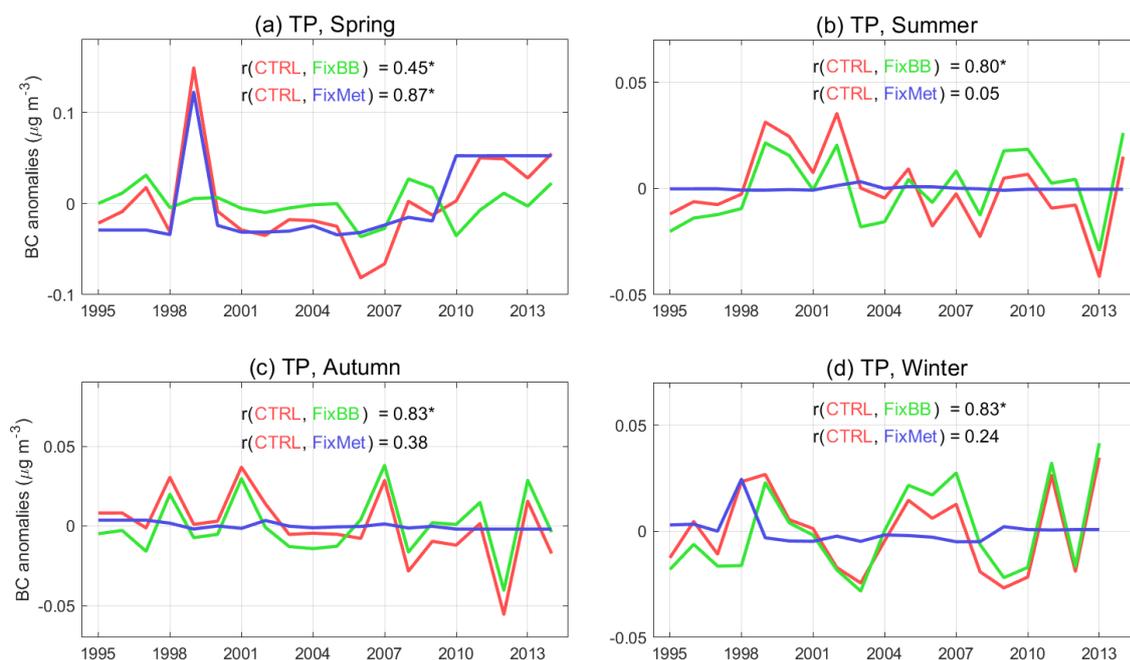
Figure 8. Interannual variations of the anomalies of surface BC concentrations averaged over the TP from different simulations during 1995-2014 in the four seasons. Red, green, and blue lines indicate CTRL, FixBB, and FixMet simulations, respectively. The anomalies are the BC concentrations in a given year minus those in the 20-year mean. A correlation coefficient (r) with '*' indicates that the r is statistically significant ($p<0.05$).

1040
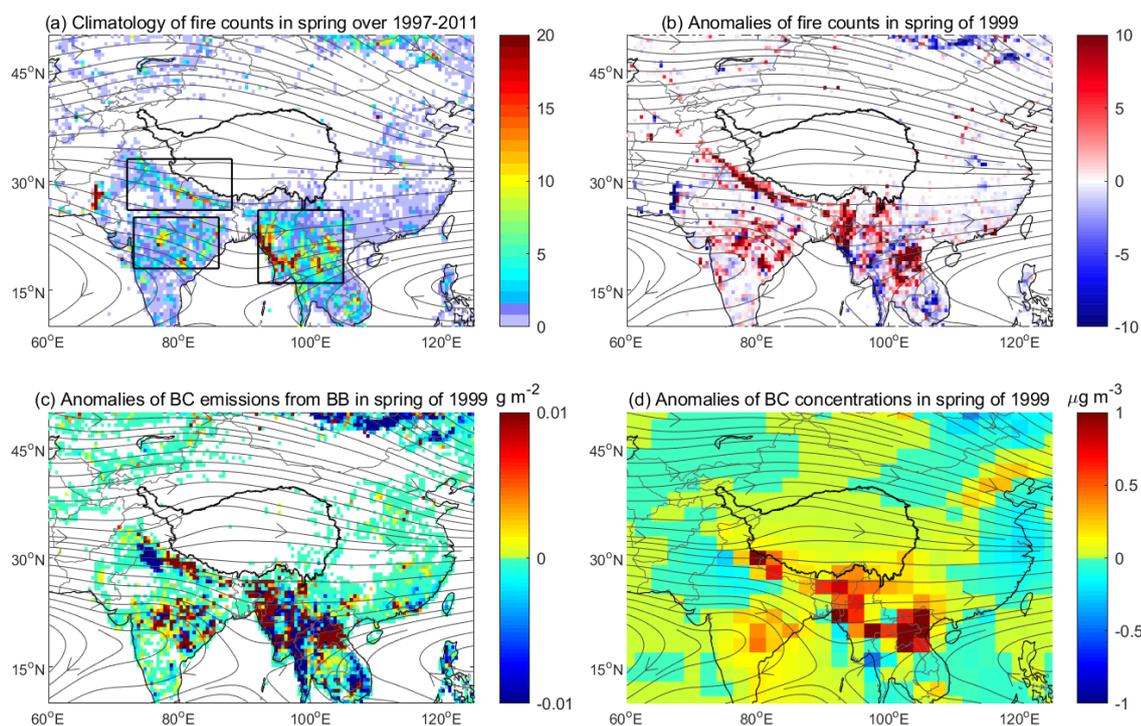
1045

Figure 9. Extremely strong biomass burning in spring of 1999 and the corresponding surface BC anomalies and wind field over the TP and surrounding regions. (a) Climatology of fire counts from ATSR in spring overlaid with streamlines at 500 hPa over 1997-2011. (b) Anomalies of fire counts from ATSR overlaid with anomalous streamlines at 500 hPa in spring of 1999. (c) The same as (b), but for the anomalies of BC emissions from biomass burning (BB) from GFED3. (d) The same as (b), but for the anomalies of BC concentrations from CTRL simulation. The anomaly in (b)-(d) is the corresponding value in 1999 minus that over 1997-2011. The boxed areas in (a) indicate the fire regions in the Indo-Gangetic Plain, central India, and Southeast Asia. The dark black line encloses the domain of the TP.
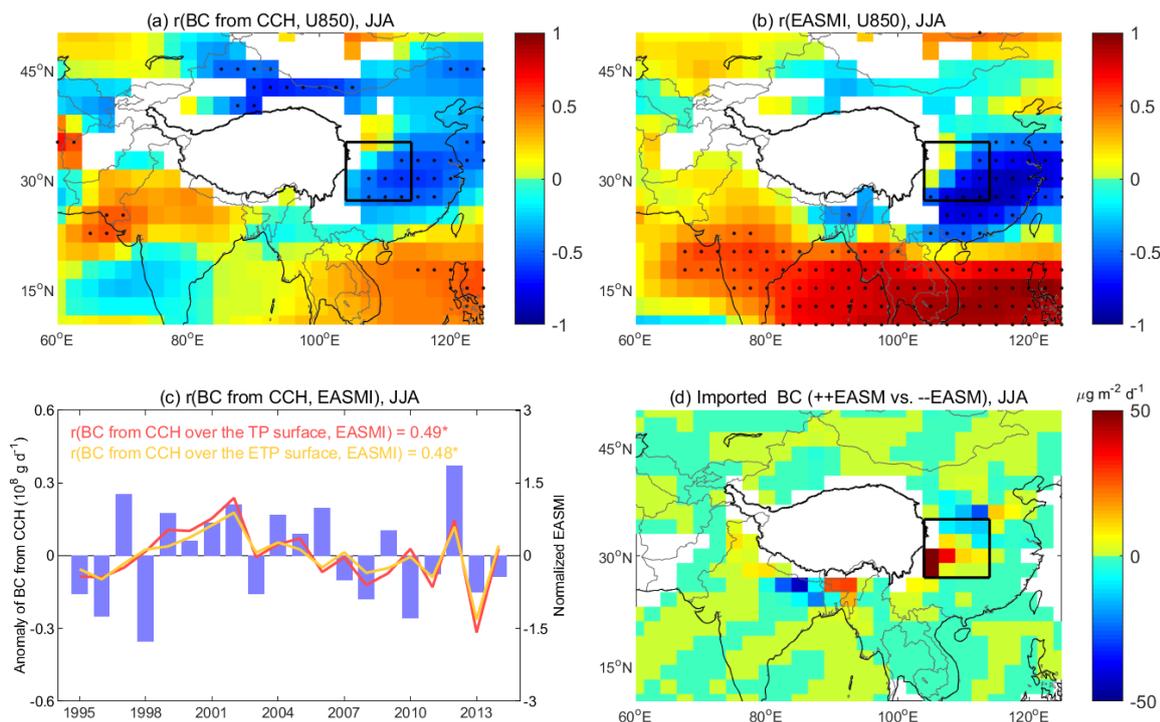
1070

1075

1080

Figure 10. Connection between BC transport from East Asia to the TP surface and the EASM in summer. (a) Correlation coefficients (r) between the zonal wind at 850 hPa (U850) and imported BC from central China (CCH) over the TP surface. (b) r between the EASMI and U850. (c) Interannual variations in the intensity of the EASM, and imported BC from CCH to the surface of the TP and eastern TP (ETP). (d) Differences in BC transport to the TP surface between the years with strong and weak EASM. Dots in (a) and (b) indicate the r in the corresponding grid is statistically significant ($p<0.05$). The unfilled grids in (a) and (b) are due to the topography. A r with '*' in (c) indicates that the r is statistically significant ($p<0.05$). Boxed areas in (a), (b), and (d) indicate CCH (see Figure 4b). The dark black line in (a), (b), and (d) encloses the domain of the TP.
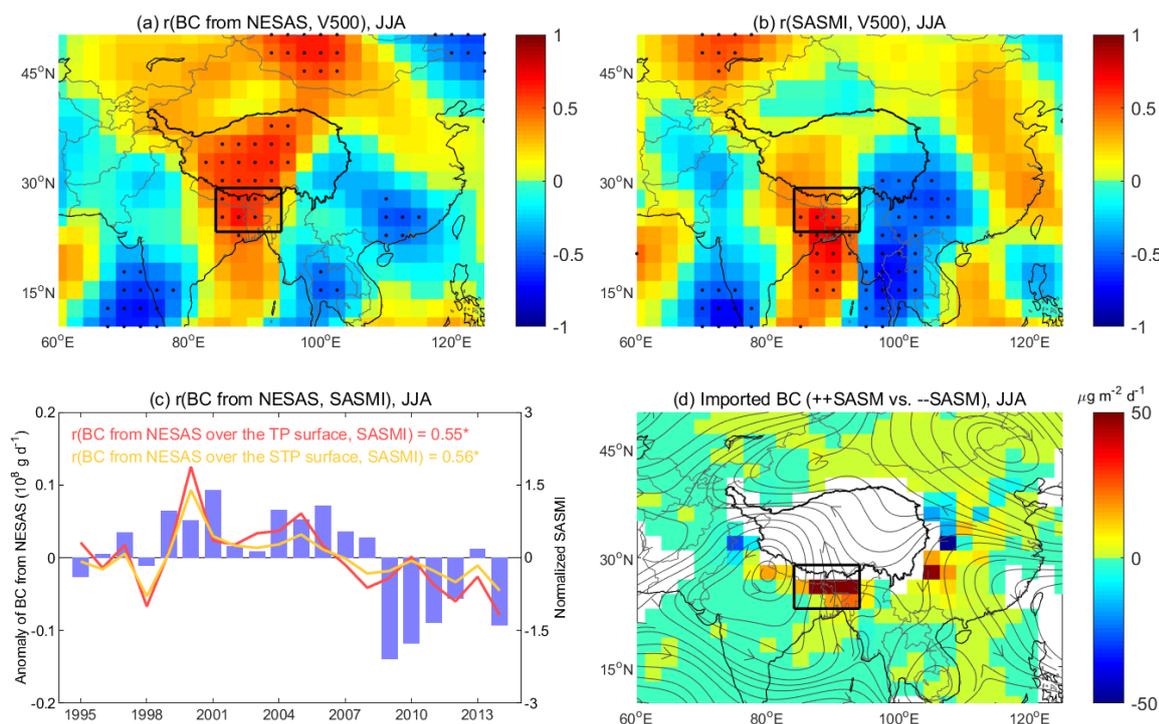
1085

1090

Figure 11. Connection between BC transport from South Asia to the TP surface and the SASM in summer. (a) Correlation coefficients (*r*) between meridional wind at 500 hPa (V500) and imported BC from northeastern South Asia (NESAS) over the TP surface. (b) *r* between the SASMI and V500. (c) Interannual variations in the intensity of the SASM, and imported BC from NESAS to the surface of the TP and southern TP (STP). (d) Differences in BC transport to the TP surface between the years with strong and weak SASM. Dots in (a) and (b) indicate the *r* in the corresponding grid is statistically significant (*p*<0.05). A *r* with '*' in (c) indicates that the *r* is statistically significant (p<0.05). Streamlines in (d) are the differences between the years with strong and weak SASM at 500 hPa. Boxed areas in (a), (b), and (d) indicate NESAS (see Figure 4b). The dark black line in (a), (b), and (d) encloses the domain of the TP.
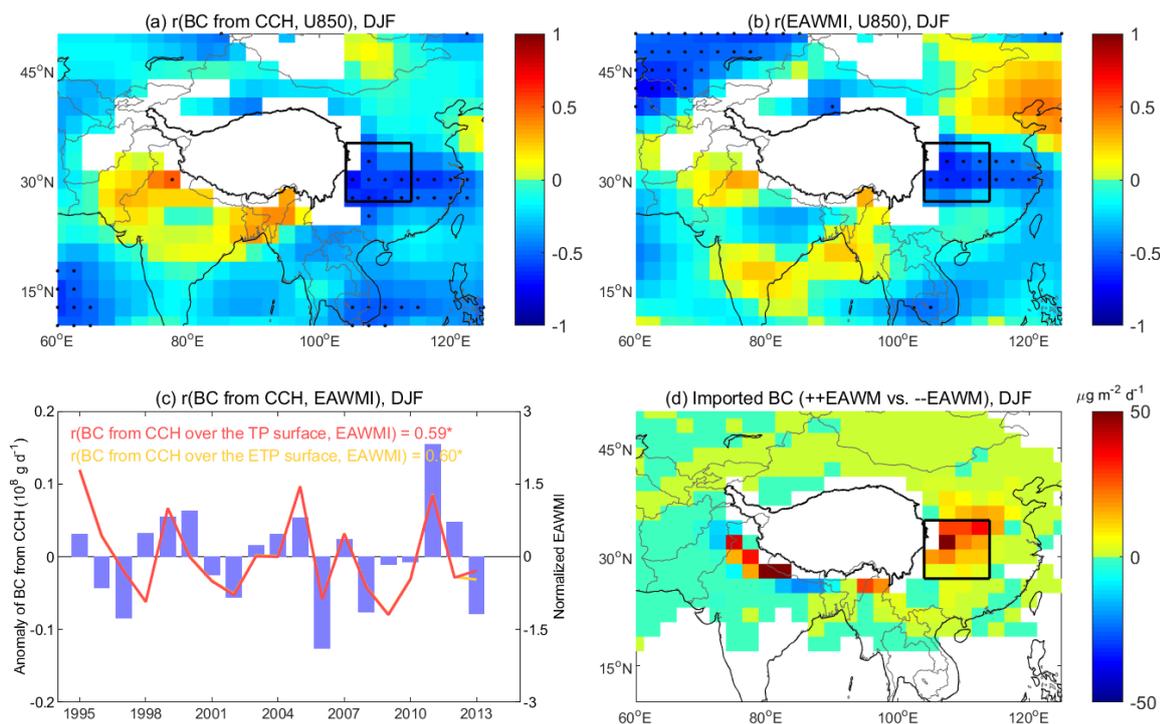
Figure 12. Connection between BC transport from East Asia to the TP surface and the EAWM in winter. (a) Correlation coefficients (r) between imported BC from central China (CCH) to surface BC in the TP and zonal wind at 850 hPa (U850). (b) r between the EAWMI and U850. (c) Interannual variations in the intensity of the EAWM, and imported BC from CCH to the surface of the TP and eastern TP (ETP). (d) Differences in BC transport to the TP surface between the years with strong and weak EAWM. Dots in (a) and (b) indicate the r in the corresponding grid is statistically significant ($p < 0.05$). The unfilled grids in (a) and (b) are due to the topography. A r with '*' in (c) indicates that the r is statistically significant ($p < 0.05$). Boxed areas in (a), (b), and (d) indicate CCH (see Figure 4d). The dark black line in (a), (b), and (d) encloses the domain of the TP.

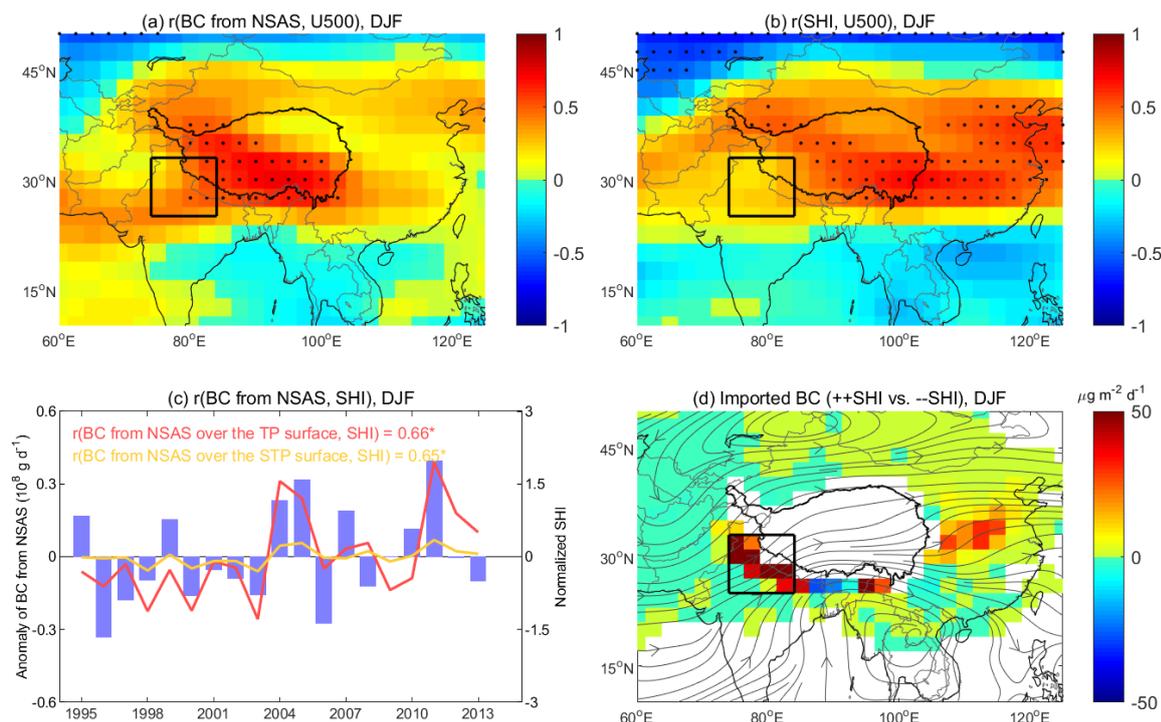Atmospheric
Chemistry
and Physics
Discussions

Figure 13. Connection between BC transport from South Asia to the TP surface and the Siberian High in winter. (a) Correlation coefficients (*r*) between zonal wind at 500 hPa (U500) and imported BC from northern South Asia (NSAS) over the TP surface. (b) *r* between the SHI and U500. (c) Interannual variations in the SHI, and imported BC from NSAS to the surface of the TP and southern TP (STP). (d) Differences in BC transport to the TP surface between the years with strong and weak Siberian High. Dots in (a) and (b) indicate the *r* in the corresponding grid is statistically significant ($p<0.05$). A *r* with '*' in (c) indicates that the *r* is statistically significant (p<0.05). Streamlines in (d) are the differences between the years with strong and weak Siberian High at 500 hPa. Boxed areas in (a), (b), and (d) indicate NSAS (see Figure 4d). The dark black line in (a), (b), and (d) encloses the domain of the TP.